iScience

CellPress
OPEN ACCESS

Article

# FGF13 Is a Novel Regulator of NF-κB and Potentiates Pathological Cardiac Hypertrophy

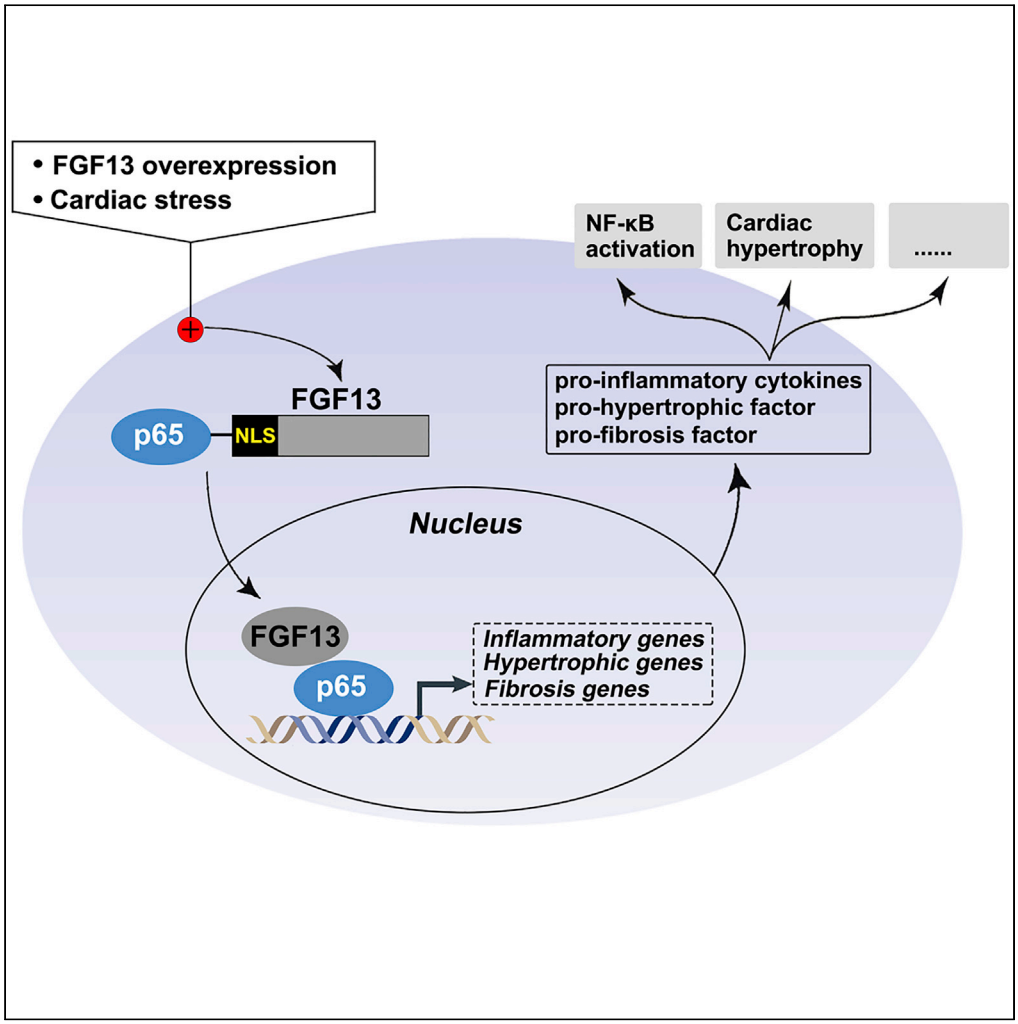


Jia Sun, Chao Niu, Weijian Ye, ..., Litai Jin, Weitao Cong, Xiaokun Li

jin_litai@126.com (L.J.)
cwt97126@126.com (W.C.)
profxiaokunli@163.com (X.L.)

## HIGHLIGHTS

Endogenous FGF13 is up-regulated in cardiomyocytes under pressure overload

FGF13 directly interacts with p65

Forced FGF13 overexpression activates NF-κB in cardiomyocytes

Sun et al., iScience *23*, 101627
October 23, 2020 
https://doi.org/10.1016/j.isci.2020.101627

iScience

CellPress
OPEN ACCESS

Article

# FGF13 Is a Novel Regulator of NF-κB and Potentiates Pathological Cardiac Hypertrophy

Jia Sun,[1,6] Chao Niu,[2,6] Weijian Ye,[3] Ning An,[1] Gen Chen,[1] Xiaozhong Huang,[4] Jianan Wang,[1] Xixi Chen,[1] Yingjie Shen,[1] Shuai Huang,[1] Ying Wang,[1] Xu Wang,[1] Yang Wang,[5] Litai Jin,[1,*] Weitao Cong,[1,*] and Xiaokun Li[1,7,*]

## SUMMARY

**FGF13 is an intracellular FGF factor. Its role in cardiomyopathies has been rarely investigated. We revealed that endogenous FGF13 is up-regulated in cardiac hypertrophy accompanied by increased nuclear localization. The upregulation of FGF13 plays a deteriorating role both in hypertrophic cardiomyocytes and mouse hearts. Mechanistically, FGF13 directly interacts with p65 by its nuclear localization sequence and co-localizes with p65 in the nucleus in cardiac hypertrophy. FGF13 deficiency inhibits NF-κB activation in ISO-treated NRCMs and TAC-surgery mouse hearts, whereas FGF13 overexpression shows the opposite trend. Moreover, FGF13 overexpression alone is sufficient to activate NF-κB in cardiomyocytes. The interaction between FGF13 and p65 or the effects of FGF13 on NF-κB have nothing to do with IκB. Together, an IκB-independent mechanism for NF-κB regulation has been revealed in cardiomyocytes both under basal and stressful conditions, suggesting the promising application of FGF13 as a therapeutic target for pathological cardiac hypertrophy and heart failure.**

## INTRODUCTION

FGF13, belonging to the fibroblast growth factor (FGF) homologous factors (FHFs), harbors a heparin-binding site but without secreted signal sequence (Olsen et al., 2003), and its orthologous variable region exons in mice and humans are highly conserved (Itoh and Ornitz, 2008). The literature typically suggests that intracellular FGF13 modulates the function of voltage-gated sodium channels (NaVs) through an FGFR-independent manner (Olsen et al., 2003). FGF13 participates in regulating the ion-gating properties and the distribution of NaVs through interacting with NaVs (Goldfarb et al., 2007; Wang et al., 2011; Xiao et al., 2013; Hsu et al., 2014; Wang et al., 2017). Also, deficiency of FGF13 suppresses cardiac sodium currents at elevated temperatures via increasing the rate of closed-state and open-state sodium channel inactivation (Park et al., 2016). The role of FGF13 in regulating cardiac function, however, has only been recently investigated. Conditional knockout of FGF13 in murine hearts increases arrhythmia susceptibility and exhibits an increased abundance of caveolae in cardiomyocytes and thereby ameliorates pathological myocardial hypertrophy (Wang et al., 2017; Wei et al., 2017). Nevertheless, the importance of FGF13 in cardiomyocytes remains to be explored.

The heart undergoes a hypertrophic response in virtually all forms of cardiomyopathies (Molkentin et al., 1998). Sustained pathological hypertrophy can finally result in heart failure and sudden death (Levy et al., 2002; Ucar et al., 2012). NF-κB is a broadly expressed transcription factor involved in regulating genes participating in innate immune response, cell survival, inflammation, and proliferation (Valen, 2004; Jones et al., 2005). Notably, NF-κB activation has been closely linked to the development of pathological cardiac hypertrophy (Purcell et al., 2001; Valen, 2004; Gupta and Sen, 2005).

Here we describe that FGF13 is a novel regulator of NF-κB in cardiomyocytes under both basal and stressful conditions. FGF13 interacts with p65 through its NLS (nuclear localization sequence) and acts an indispensable role in regulating NF-κB activation, suggesting a unique strategy for intervening in NF-κB. This study will provide new perspectives in studying FHFs in heart-related diseases.

[1]School of Pharmaceutical Science, Wenzhou Medical University, Wenzhou 325000, China

[2]Pediatric Research Institute, The Second Affiliated Hospital and Yuying Children's Hospital of Wenzhou Medical University, Wenzhou 325000, China

[3]Department of Pharmacy, The Second Affiliated Hospital and Yuying Children's Hospital of Wenzhou Medical University, Wenzhou 325000, China

[4]Department of Pediatric Surgery, The Second Affiliated Hospital and Yuying Children's Hospital of Wenzhou Medical University, Wenzhou 325000, China

[5]Department of Histology and Embryology, Institute of Neuroscience, Wenzhou Medical University Wenzhou, 325000, China

[6]These authors contributed equally

[7]Lead Contact

*Correspondence: jin_litai@126.com (L.J.), cwt97126@126.com (W.C.), profxiaokunli@163.com (X.L.)

https://doi.org/10.1016/j.isci.2020.101627

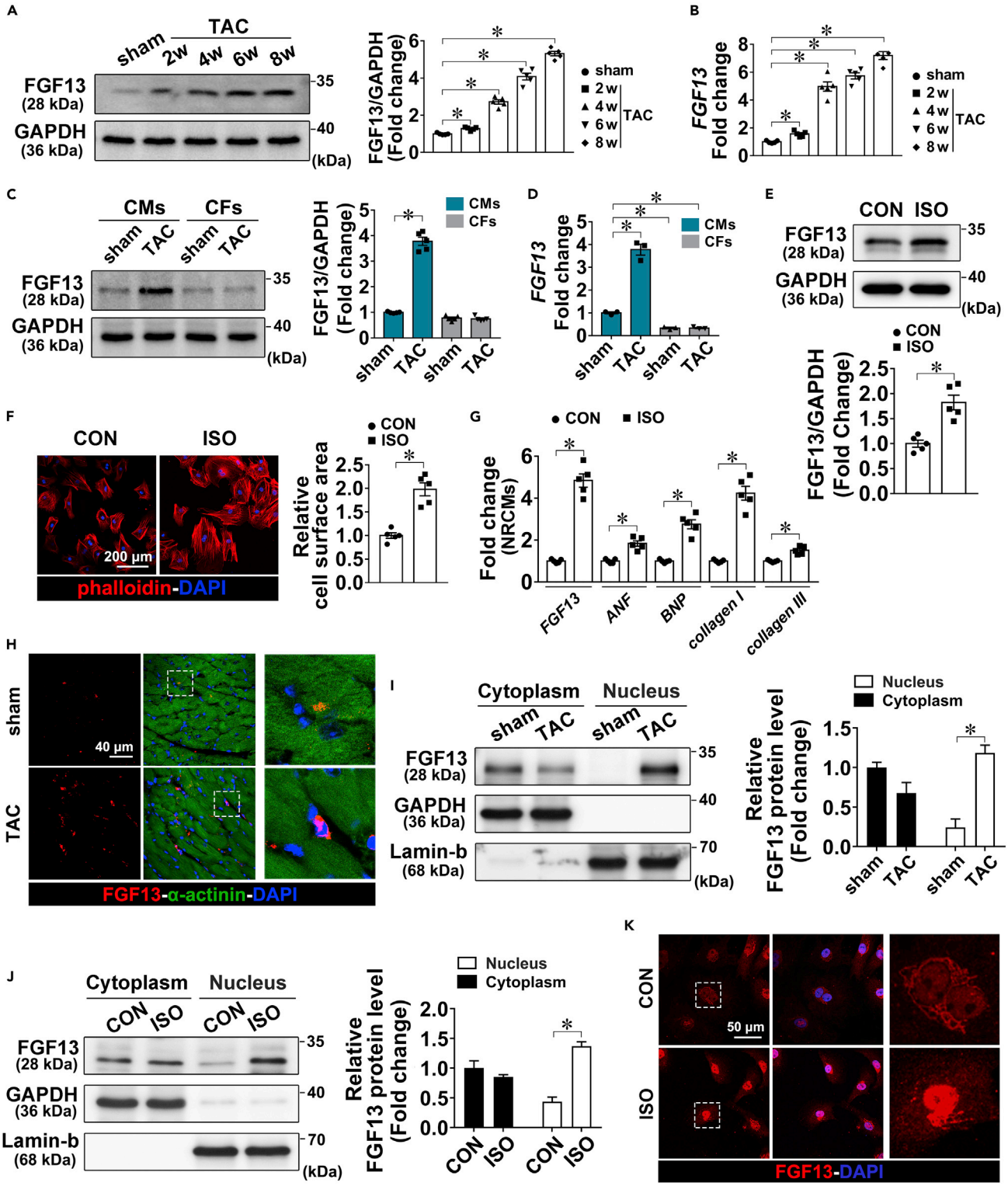


**Figure 1. Endogenous FGF13 Is Up-regulated in Cardiac Hypertrophy Accompanied by Its Nuclear Accumulation**

(A) Western blot analysis and quantification of the FGF13 protein level (n = 5 per group).

(B) qRT-PCR analysis of *FGF13* mRNA level in mouse hearts (n = 5 per group).

(C) Western blot analysis and quantification of the FGF13 protein level in CMs and non-CMs isolated from sham and TAC surgery (4 weeks) mouse hearts (n = 5 per group).

**Figure 1. *Continued***
(D) qRT-PCR analysis of *FGF13* mRNA level in mouse hearts in the same groups as (C) (n = 5 per group).
(E) Western blot analysis and quantification of the FGF13 protein level in NRCMs (n = 5 per group).
(F) Representative images of Phalloidin (red) and DAPI (blue)-stained NRCMs (n = 5 per group).
(G) qRT-PCR analysis of FGF13, the hypertrophic marker genes (*ANF, BNP*), fibrotic marker genes (*collagen I, collagen III*) in NRCMs (n = 5 per group).
(H) IF staining for FGF13 (red) counterstained with α-actinin (green) to measure the subcellular localization of FGF13 on heart sections (n = 5 per group).
Western blot analysis and quantification of the subcellular localization of endogenous FGF13 in mouse hearts (I), or NRCMs (J) (n = 5 per group).
(K) Representative confocal images of subcellular localization of endogenous FGF13 in NRCMs (n = 5 per group).
Data are presented as mean ± SEM. *p < 0.05 represents statistically significant differences.

## RESULTS

### Endogenous FGF13 Is Up-Regulated in Pressure Overload-Induced Cardiac Hypertrophy Accompanied by Its Nuclear Accumulation

In order to explore the latent role of FGF13 in pressure overload-induced cardiac hypertrophy, we first confirmed whether the FGF13 expression level was changed in response to pressure overload. Both the protein and mRNA levels of FGF13 were progressively increased in mice at 2, 4, 6, and 8 weeks after receiving TAC (Transverse Aortic Constriction) surgery compared with the sham surgery mice (Figures 1A and 1B). We next confirmed the specific cell types of the high expressed FGF13 in sham or TAC surgery (4 weeks) mouse hearts. FGF13 was predominantly increased in cardiomyocytes (CMs), rather than other cell types such as cardiac fibroblasts (CFs) isolated from sham and TAC surgery mouse hearts (Figures 1C, 1D, and S1). Meanwhile, ISO (Isoproterenol) was used to construct the *in vitro* model of cardiac hypertrophy in NRCMs (Neonatal Rat Cardiomyocytes) (Simpson, 1985). The increased FGF13 level was confirmed in ISO-treated NRCMs (Figure 1E), along with the increased cell size as assessed by Phalloidin staining (Figure 1F) and increased transcriptional levels of hypertrophic marker genes (*ANF*, *BNP*) and fibrotic markers (*Collagen I*, *Collagen III*) (Figure 1G).

Next, we sought to determine the subcellular distribution of FGF13 in response to pressure overload. IF (immunofluorescence) staining showed that FGF13 was mostly localized in the cytoplasm in sham surgery mouse hearts, whereas a remarkable nuclear accumulation was detected in TAC surgery mouse hearts (Figure 1H), which were further confirmed by western blot analysis (Figure 1I). Consistently, ISO-treated NRCMs showed the similar trend of FGF13 nuclear localization (Figures 1J and 1K).

FGF13 transcript variants generate five different isoforms that have tissue-specific expression patterns and different subcellular distributions. Accordingly, we investigated which FGF13 transcripts were most abundant in CMs isolated from sham and TAC surgery mouse hearts. sqRT-PCR (semi-quantitative reverse transcriptase PCR) and qRT-PCR (quantitative real-time reverse transcription PCR) assays with isoform-specific primers were used to define the relative expressions of five FGF13 isoforms in CMs. The relative mRNA expression levels showed that FGF13-S mRNA level was significantly higher in CMs isolated from TAC-surgery mouse hearts than in CMs isolated from sham-surgery mouse hearts. The differences observed for the other variants (FGF13-U, FGF13-V, FGF13-Y, and FGF13-VY) between the two groups were minimal (Figures S2A and S2B).

### FGF13 Participates in Pressure Overload-Induced Cardiac Hypertrophy

To determine the exact role of FGF13 in the process of cardiac hypertrophy, we constructed an adenovirus harboring FGF13 short hairpin RNA (shRNA) (Ad-shFGF13) to genetically knockdown FGF13 expression in NRCMs (Figure S2C). We found that FGF13 downregulation in ISO-treated NRCMs caused a significant decrease in cell size (Figure 2A) and the mRNA levels of hypertrophic marker genes (*ANF*, *BNP*), fibrotic genes (*Collagen I*, *Collagen III*), and inflammatory genes (*IL-6*, *IL-1β*) compared with the Ad-Scramble transfected NRCMs (Figure 2B).

Meanwhile, AAV9-shFGF13 was used to knockdown FGF13 in CMs in mouse hearts, which were then exposed to TAC-surgery for 4 weeks (Figure S2D). The delivery was confirmed by western blot (Figure S2E). Compared with the AAV-Scramble-treated mouse, FGF13 knockdown mouse showed no significant differences in heart phenotype or cardiac function at baseline (Figures S2F–S2N). Notably, knockdown of FGF13 significantly decreased the ratios of heart weight to body weight (HW/BW) and the ratios of heart weight to tibia length (HW/TL) under pressure overload. Also, FGF13 deficiency increased the ejection fraction (EF) and fractional shortening (FS) compared with the mice injected with AAV9-Scramble in TAC surgery hearts

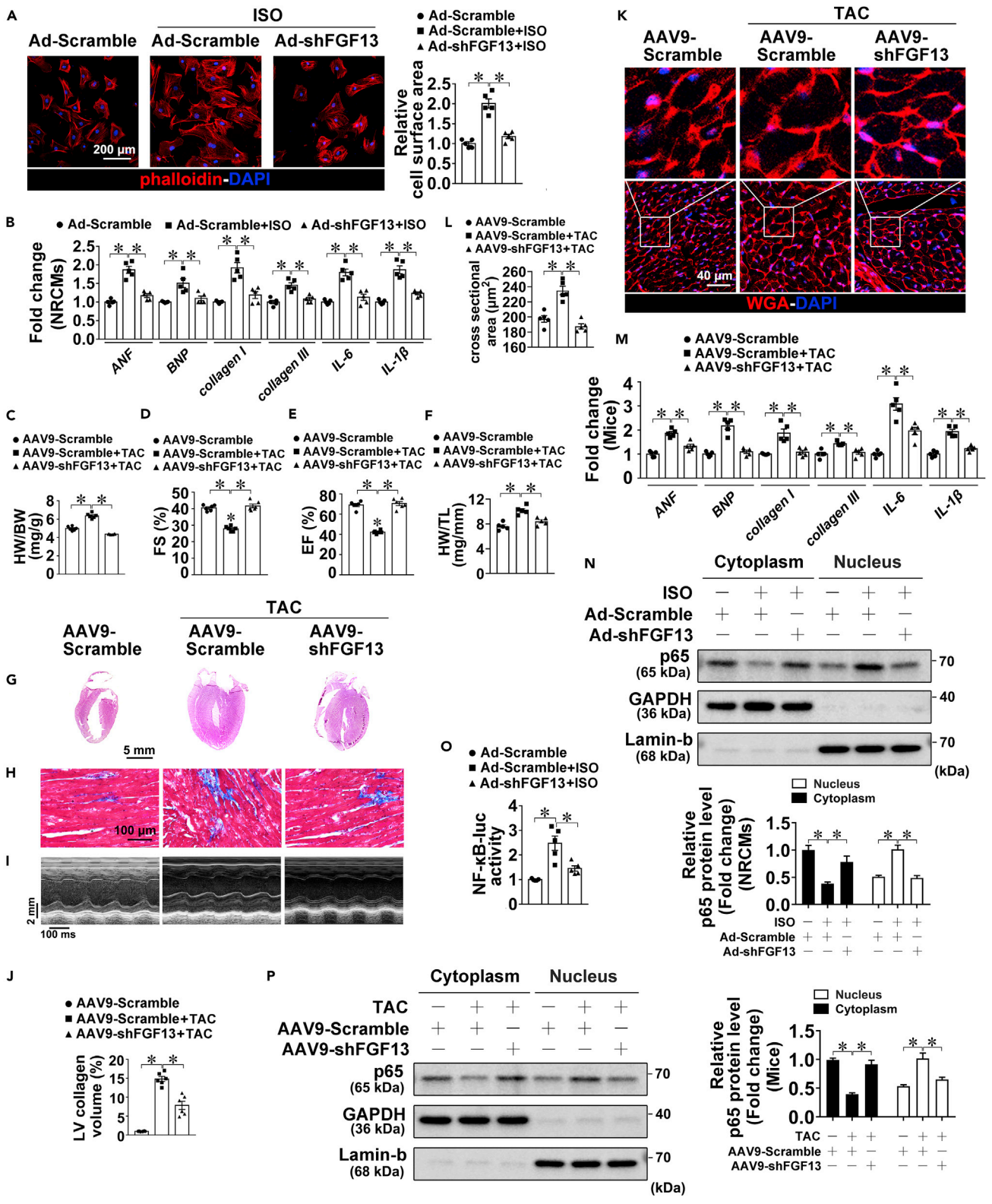
A
ISO
Ad-Scramble
Ad-Scramble
Ad-shFGF13
200 μm
phalloidin-DAPI
● Ad-Scramble
■ Ad-Scramble+ISO
▲ Ad-shFGF13+ISO
Relative cell surface area
B
● Ad-Scramble ■ Ad-Scramble+ISO ▲ Ad-shFGF13+ISO
Fold change (NRCMs)
ANF
BNP
collagen I
collagen III
IL-6
IL-1β
L
● AAV9-Scramble
■ AAV9-Scramble+TAC
▲ AAV9-shFGF13+TAC
cross sectional area (μm²)
C
● AAV9-Scramble
■ AAV9-Scramble+TAC
▲ AAV9-shFGF13+TAC
HW/BW (mg/g)
D
● AAV9-Scramble
■ AAV9-Scramble+TAC
▲ AAV9-shFGF13+TAC
FS (%)
E
● AAV9-Scramble
■ AAV9-Scramble+TAC
▲ AAV9-shFGF13+TAC
EF (%)
F
● AAV9-Scramble
■ AAV9-Scramble+TAC
▲ AAV9-shFGF13+TAC
HW/TL (mg/mm)
K
TAC
AAV9-Scramble
AAV9-Scramble
AAV9-shFGF13
40 μm
WGA-DAPI
M
● AAV9-Scramble
■ AAV9-Scramble+TAC
▲ AAV9-shFGF13+TAC
Fold change (Mice)
ANF
BNP
collagen I
collagen III
IL-6
IL-1β
TAC
AAV9-Scramble
AAV9-Scramble
AAV9-shFGF13
G
5 mm
H
100 μm
I
2 mm
100 ms
N
Cytoplasm
Nucleus
ISO
Ad-Scramble
Ad-shFGF13
p65 (65 kDa)
GAPDH (36 kDa)
Lamin-b (68 kDa)
(kDa)
Nucleus
Cytoplasm
Relative p65 protein level (Fold change) (NRCMs)
O
● Ad-Scramble
■ Ad-Scramble+ISO
▲ Ad-shFGF13+ISO
NF-κB-luc activity
J
● AAV9-Scramble
■ AAV9-Scramble+TAC
▲ AAV9-shFGF13+TAC
LV collagen volume (%)
P
Cytoplasm
Nucleus
TAC
AAV9-Scramble
AAV9-shFGF13
p65 (65 kDa)
GAPDH (36 kDa)
Lamin-b (68 kDa)
(kDa)
Nucleus
Cytoplasm
Relative p65 protein level (Fold change) (Mice)

**Figure 2. Inhibition Targeting of FGF13 Ameliorated the Detrimental Effects of Pressure Overload**

(A) Representative images of Phalloidin (red) and DAPI (blue)-stained NRCMs (n = 5 per group).
(B) qRT-PCR analysis of the hypertrophic marker genes (*ANF*, *BNP*), fibrotic marker genes (*collagen I*, *collagen III*), and NF-κB targeted proinflammatory genes (*IL-6*, *IL-1β*) (n = 5 per group).
(C) Postmortem measurements of HW/BW (mg/g) after 4 weeks of sham or TAC surgery (n = 6 per group).
(D and E) Measurement of FS (%) and EF (%) (n = 6 per group).
(F) Postmortem measurements of HW/TL (mg/mm) (n = 5 per group).
(G) Sagittal sections of mouse hearts stained with H&E (n = 6 per group).
(H) Heart sections stained with Masson (n = 6 per group).
(I) Representative echocardiograms (n = 6 per group).
(J) Quantification of the LV collagen volume in (H).
(K) IF staining for WGA (red) (n = 5 per group).
(L) Quantification of the cross-sectional area in (K).
(M) qRT-PCR analysis of the *ANF, BNP, collagen I, collagen III, IL-6, IL-1β* (n = 5 per group).
(N) Western blot analysis and quantification of the p65 in cytoplasmic and nuclear extracts (n = 5 per group).
(O) NF-κB luciferase reporter assay (n = 5 per group).
(P) Western blot analysis and quantification of p65 in cytoplasmic and nuclear extracts (n = 5 per group).
Data are presented as mean ± SEM. *p < 0.05 represents statistically significant differences.

(Figures 2C–2F). Furthermore, the TAC-operated FGF13 knockdown mice exhibited reduced ventricular wall thickness (Figures 2G and 2I), interstitial fibrosis (Figures 2H and 2J), and cardiomyocyte cross-section area (Figures 2K and 2L). In parallel, the transcription levels of related genes (*ANF*, *BNP*, *Collagen I*, *Collagen III*, *IL-6*, *IL-1β*) were all decreased in the TAC-operated FGF13 knockdown mice (Figure 2M) compared with those of TAC surgery mice. These findings are consistent with previous research documenting the cardioprotection in FGF13 knockout mice during pressure overload (Wei et al., 2017).

NF-κB signaling pathway has been implicated as a critical regulator of pathological cardiac hypertrophy (Purcell et al., 2001; Gupta and Sen, 2005; Suckau et al., 2009). Based on our findings that inflammatory genes were down-regulated after FGF13 ablation, we thus explored whether FGF13 played a role in NF-κB activation under pressure overload. Under resting conditions, inactive NF-κB dimers (classically p65/p50) are bound to inhibitor of κB (IκB) in the cytoplasm. NF-κB activation is typically regulated by its nuclear translocation (Hall et al., 2006). Herein, western blot analysis showed increased nuclear translocation of NF-κB p65 in ISO-treated NRCMs, whereas the specific abrogation of FGF13 resulted in a general redistribution of p65 protein to the cytoplasm (Figure 2N). In addition, NF-κB luciferase activity induced by ISO was largely blocked in FGF13 downregulated NRCMs (Figure 2O), as well as the decreased IL-6 and IL-1β protein levels (Figure S3A). Similar results were obtained in *in vivo* experiments. Compared with the sham operation, the pressure overload caused obvious nuclear translocation of p65, which was downplayed in FGF13 deficiency mice (Figure 2P). Besides, FGF13 downregulation could antagonize the transcription and translation of NF-κB p65-targeted inflammatory genes (Figures 2M and S3B). Additionally, immunoblotting for NF-κB p50 in cytosolic and nuclear extracts revealed a little bit less (diminished) p50 nuclear translocation in hypertrophic NRCMs and hearts. However, FGF13 deficiency in myocytes did not impact the p50 nuclear translocation (Figures S3C and S3D).

Diverse studies suggest that NF-κB serves as a control point that can induce either survival or death depending on the cell type and nature of the stimulus. Hence, we examined whether deficiency of FGF13 impaired NF-κB activation could affect cardiac cell death. The results showed that inhibition of FGF13 diminished TAC surgery-induced apoptosis, as evidenced by decreased ratio of Bax/Bcl-2, decreased expression level of c-Caspase 3, and reduced TUNEL positive cells (Figures S3F and S3G). Similar results were obtained in NRCMs (Figure S3E). These results indicated that FGF13 ablation reduced pressure overload-induced NF-κB activation and cell death. Also, we verified if FGF13 influences calcineurin signaling, the pathway associated with pathophysiological remodeling (Konhilas et al., 2006). In FGF13 knockdown mice subjected to TAC, we assessed calcineurin activity by measuring the expression of regulator of calcineurin 1 (Rcan1), a gene target of calcineurin (Kreusser et al., 2014). FGF13 knockdown significantly attenuated the TAC-induced increase in Rcan1 expression. Consistently, FGF13 deficiency in NRCMs inhibited ISO-induced elevated Rcan1 expression (Figure S3H). Additionally, we also examined the role of FGF13 and NF-κB signaling on the physiological hypertrophy. After swimming training, a significant increase in the cardiac cross-sectional area was observed in the exercise group as compared with sedentary control animals without myocardial interstitial fibrosis (Figures S3I–S3K). Interestingly, moderate exercise significantly suppresses NF-κB signaling in the hearts, as reflected by the decrease in p-IκBα and the increase

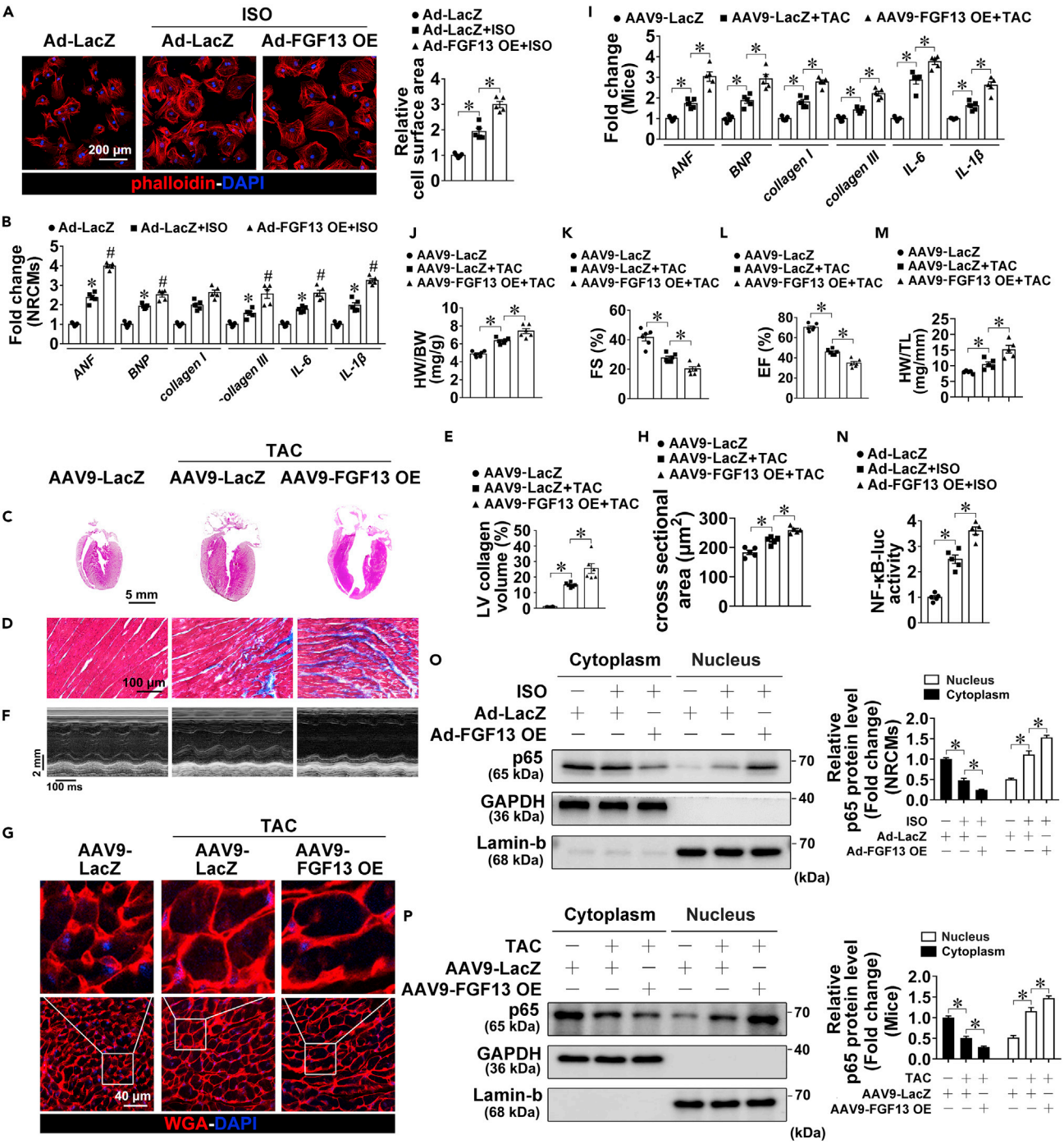


**Figure 3. FGF13 OE Exacerbated Pathological Cardiac Hypertrophy**

(A) Representative images of Phalloidin (red) and DAPI (blue)-stained NRCMs (n = 5 per group).

(B) qRT-PCR analysis of the hypertrophic marker genes (*ANF*, *BNP*), fibrotic marker genes (*collagen I*, *collagen III*), and NF-κB targeted proinflammatory genes (*IL-6*, *IL-1β*) (n = 5 per group). *p < 0.05 vs. Ad-LacZ; #p < 0.05 vs. Ad-LacZ+ISO.

(C) Sagittal sections of mouse hearts stained with H&E (n = 5 per group).

(D) Heart sections stained with Masson (n = 6 per group).

(E) Quantification of the LV collagen volume in (D).

(F) Representative echocardiograms (n = 6 per group).

(G) IF staining for WGA (red) in mouse hearts (n = 5 per group).

(H) Quantification of the cross-sectional area in (G).

**Figure 3. *Continued***

(I) qRT-PCR analysis of the *ANF*, *BNP*, *collagen I*, *collagen III*, *IL-6*, *IL-1β* in mouse hearts (n = 5 per group).
(J) Postmortem measurements of HW/BW (mg/g) after 4 weeks of sham or TAC surgery (n = 6 per group).
(K and L) Measurement of FS (%) and EF (%) (n = 6 per group).
(M) Postmortem measurements of HW/TL (mg/mm) (n = 5 per group).
(N) NF-κB luciferase reporter assay (n = 5 per group).
(O) Western blot analysis and quantification of p65 in cytoplasmic and nuclear extracts prepared in NRCMs (n = 5 per group).
(P) Western blot analysis of p65 in cytoplasmic and nuclear extracts prepared in mouse hearts (n = 5 per group).
Data are presented as mean ± SEM. *p < 0.05 represents statistically significant differences.

of IκBα protein level; decreased IL-6, IL-1β protein levels; as well as decreased nuclear p65 localization. However, FGF13 showed no obvious differences between the sedentary control and exercise mouse hearts (Figures S3L and S3M).

To exclude the possibility that the upregulation of FGF13 is a compensatory mechanism under pressure overload, we constructed an FGF13 overexpression system (Ad-FGF13 OE) in NRCMs (Figure S4A). Compared with ISO-treated NRCMs, the phalloidin staining assay indicated that FGF13 OE further increased cell size (Figure 3A). In addition, hypertrophic marker genes (*ANF*, *BNP*), fibrotic markers (*Collagen I*, *Collagen III*), and inflammatory genes (*IL-6*, *IL-1β*) (Figure 3B) in FGF13-overexpressed cells were much higher than in ISO-treated NRCMs. Similar to the results *in vitro*, FGF13 OE in hypertrophic mice (Figure S4B) further promoted cardiac fibrosis (Figures 3D and 3E) and increased the expression of marker genes, including *ANF, BNP, Collagen I, Collagen III, IL-6, and IL-1β* (Figure 3I). Moreover, FGF13 OE in hypertrophic mice sensitized the mice to pressure overload challenge, as evidenced by an increase in HW/BW, HW/TL, and the left ventricular diameter, a thinning of the left ventricular free wall, as well as a sudden reduction in the EF and FS compared with the mice after TAC-surgery for 4 weeks (Figures 3C–3H and 3J–3M). These findings suggest that the upregulation of FGF13 plays a deleterious role in hypertrophic mouse hearts.

Additionally, FGF13 OE in ISO-treated NRCMs further strengthened the NF-κB activation compared with the hypertrophic NRCMs (Figures 3N, 3O, and S4C). We also confirmed the regulatory role of FGF13 in NF-κB activation in FGF13 overexpressed mouse hearts. The upregulated IL-6, IL-1β protein levels and nuclear translocation of NF-κB p65 and NF-κB luciferase activity after TAC-surgery were all significantly aggravated (Figures 3I, 3P, and S4D). These data indicate that FGF13 serves as a positive regulator of NF-κB activity under pressure overload.

## FGF13 Regulates NF-κB Activation under Pressure Overload via an IκB-Independent Manner

We next questioned how FGF13 facilitates NF-κB activation in response to pressure overload. NF-κB activation is tightly regulated by the cellular inhibitor of κB (IκB), such as IκBα and IκBβ (Barnes and Karin, 1997; Ghosh and Baltimore, 1990; Karin, 1999). Consistent with previous studies, ISO treatment in NRCMs activated the canonical NF-κB pathway (Brown et al., 1995; DiDonato et al., 1996), as reflected by the increase in phosphorylation level of IκBα and the decrease of IκBα protein level (Figure 4A), as well as the increase in phosphorylation level of IκBβ (Figure S5A). However, FGF13 deficiency or overexpression exerted no effects on IκB (Figures 4A and S5A). In parallel, the *in vivo* results showed that the expression of phosphorylated IκBα was dramatically increased, accompanied by its degradation in the TAC-surgery mice, which was unaffected by FGF13 deficiency or overexpression (Figure S5B). Additionally, overexpression of IκBα (Figure S5C) hardly exhibited any obvious change in p65 nuclear translocation (Figure 4B) and NF-κB luciferase activity (Figure 4C) in FGF13 OE NRCMs. Moreover, the expression of NF-κB p65-targeted inflammatory genes, hypertrophic marker genes, and fibrotic genes (Figure 4D), as well as the IL-6 and IL-1β protein levels (Figure S5D) and the cell size (Figure 4E), was also unaffected as compared with FGF13 OE hypertrophic NRCMs. These results indicated that the effects of FGF13 in regulating NF-κB under pressure overload were independent of the phosphorylation or degradation of IκB.

To further evaluate the indispensable role of FGF13 in regulating NF-κB activation in response to cardiac hypertrophy, we infected NRCMs with Ad-p65 OE in the presence or absence of Ad-shFGF13, followed by the treatment of ISO for 48 h. Our results demonstrated that p65 OE worsened the hypertrophy under pressure overload conditions. Interestingly, the FGF13 deficiency reversed the effects of p65 OE on worsening cardiac hypertrophy, evidenced by a decreased cardiomyocyte size (Figures 4F and 4G). Also, FGF13

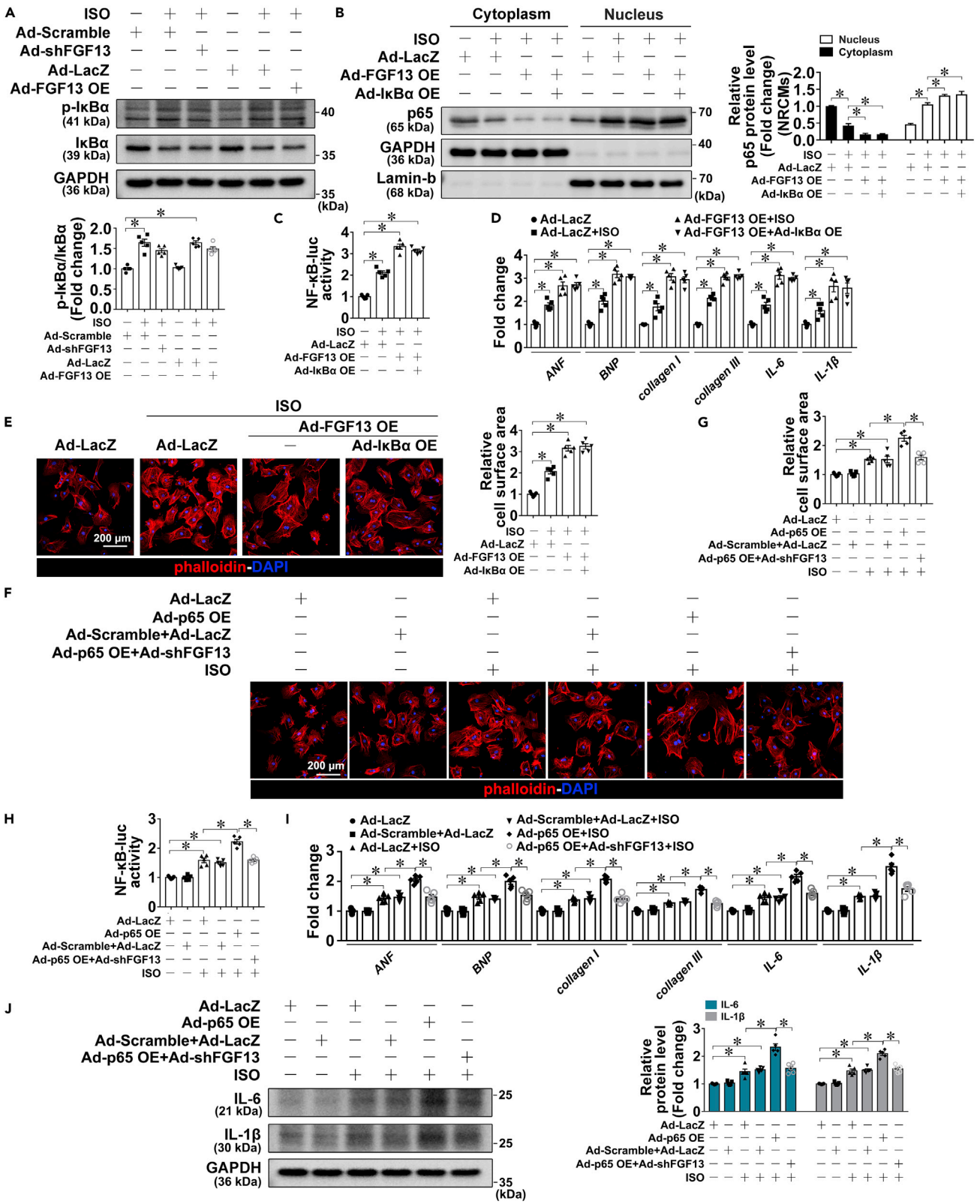
A
ISO
Ad-Scramble
Ad-shFGF13
Ad-LacZ
Ad-FGF13 OE
p-IκBα (41 kDa)
IκBα (39 kDa)
GAPDH (36 kDa)
40
35
35 (kDa)
p-IκBα/IκBα (Fold change)
B
Cytoplasm
Nucleus
Ad-IκBα OE
p65 (65 kDa)
GAPDH (36 kDa)
Lamin-b (68 kDa)
70
40
70
(kDa)
Relative p65 protein level (Fold change)
Nucleus
Cytoplasm
(NRCMs)
C
NF-κB-luc activity
D
Ad-LacZ
Ad-LacZ+ISO
Ad-FGF13 OE+ISO
Ad-FGF13 OE+Ad-IκBα OE
Fold change
ANF
BNP
collagen I
collagen III
IL-6
IL-1β
E
Ad-LacZ
Ad-IκBα OE
200 μm
phalloidin-DAPI
Relative cell surface area
G
Ad-p65 OE
Ad-Scramble+Ad-LacZ
Ad-p65 OE+Ad-shFGF13
F
H
I
Ad-Scramble+Ad-LacZ+ISO
Ad-p65 OE+ISO
Ad-p65 OE+Ad-shFGF13+ISO
J
IL-6 (21 kDa)
IL-1β (30 kDa)
25
25
35 (kDa)
IL-6
IL-1β

**Figure 4. FGF13 Is Indispensable for Regulating NF-κB Activation in Response to Cardiac Hypertrophy**

(A) Western blot analysis and quantification of p-IκBα and IκBα in cultured NRCMs (n = 5 per group).
(B) Western blot analysis and quantification of p65 in cytoplasmic and nuclear extracts prepared from NRCMs (n = 5 per group).
(C) NF-κB luciferase reporter assay (n = 5 per group).
(D) qRT-PCR analysis of the *ANF, BNP, collagen I, collagen III, IL-6, IL-1β* (n = 5 per group).
(E) Representative images of Phalloidin (red) and DAPI (blue)-stained NRCMs (n = 5 per group).
(F) Representative images of Phalloidin (red) and DAPI (blue)-stained NRCMs.
(G) Quantification of the relative cell surface area in (F).
(H) NF-κB luciferase reporter assay (n = 5 per group).
(I) qRT-PCR analysis of the *ANF, BNP, collagen I, collagen III, IL-6, IL-1β* in NRCMs (n = 5 per group).
(J) Western blot analysis and quantification of IL-6 and IL-1β in cultured NRCMs (n = 5 per group).
Data are presented as mean ± SEM. *p < 0.05 represents statistically significant differences.

deficiency blocked NF-κB luciferase activity in p65 overexpressed NRCMs and decreased mRNA levels of several genes and IL-6, IL-1β protein levels (Figures 4H–4J).

## FGF13 Interacts with p65 and Co-Localizes to p65 in the Nucleus in Response to Pressure Overload

In mouse hearts, we verified the interaction between FGF13 and p65 by co-immunoprecipitation (coIP) and confocal microscopy (Figures 5A and 5B). To confirm whether FGF13 competed with IκBα for p65 binding, the cell lysates of NRCMs were first immunoprecipitated with increasing dosage of anti-IκBα antibody and the unbound fractions were followed by reimmunoprecipitation with the anti-FGF13 antibody. Then, the immunocomplexes from both steps were analyzed by immunoblotting with IκBα, p65, and FGF13. The results showed that p65 interacted with IκBα in a dose-dependent manner. Moreover, it was concluded that the amount of anti-IκBα antibody was enough to precipitate almost all the IκBα-bound p65 in the NRCMs lysates, ascribed to the similar western blot intensity of p65 immunoprecipitated by two different amounts of anti-IκBα antibody (5 and 8 μL) (Figure S6A), and almost no remaining IκBα expression in the unbound fractions after one step of IP (Figure S6C). Interestingly, a considerable amount of p65 from the unbound fractions was immunoprecipitated with anti-FGF13, suggesting that only a part of p65 was associated with IκBα. Also, ISO-treated NRCMs shared the similar situation (Figure S6B). Furthermore, we infected NRCMs with Ad-scramble or Ad-shp65 under basal or stressful conditions for the immunoprecipitation assay (Figure S6D). Indeed, we hardly found the interaction between IκBα and FGF13 in the absence of p65 (Figure S6E), indicating that FGF13 only interacted with p65 rather than forming a complex with IκBα and p65. Consistent with this notion, we demonstrated that the interaction between FGF13 and p65 was not changed in response to specific IκBα downregulated or overexpressed NRCMs both under basal and stressful conditions (Figures S6F and S6G). In addition, SPR (surface plasmon resonance) assay demonstrated that IκBα does not interact with FGF13 (Figure S6H). These data confirmed that FGF13 interacted with p65 via an IκB-independent manner.

Next, we assessed the relationship between the nuclear translocation of FGF13 and p65 upon cardiac hypertrophy. In detail, FGF13 interacted with p65 in the cytoplasm under normal condition, whereas the complex was greatly accumulated in the nucleus along with sharp increased expression of FGF13 in ISO-stimulated NRCMs (Figure 5C). Furthermore, IF assay indicated the interaction between FGF13 and p65 (Figure 5D). The direct interaction between FGF13 and p65 was further confirmed by an SPR assay (Figure S6H).

To demonstrate the central roles of FGF13-p65 interaction in regulating cardiac hypertrophy, we infected NRCMs with Ad-FGF13 OE in the presence or absence of Ad-shp65, followed by the treatment of ISO for 48 h. p65 deficiency in ISO-treated NRCMs infected with Ad-FGF13 OE caused a significant decrease in the cell surface area and the mRNA expression levels of hypertrophic and fibrotic genes, compared with the ISO-treated NRCMs infected with Ad-FGF13 OE (Figures 5E and 5F). In parallel, AAV-FGF13 OE alone or in combination with AAV-shp65 (Figure S6I) was injected into hearts, then the mouse was subjected to TAC surgery. Histological analysis of ventricle sections stained with Masson's trichrome demonstrated decreased fibrosis in the mice injected with AAV-FGF13 OE and AAV-shp65 compared with the mice injected with AAV-FGF13 OE, whereas the narrow of the heart and cardiomyocytes were identified via H&E and WGA (Wheat Germ Agglutinin) staining assays (Figures 5G–5I and 5P). Echocardiographic data suggested that p65 deficiency improved cardiac function in the hypertrophic mice injected with AAV-FGF13 OE, as reflected by the decreased ratios of HW/BW, HW/TL, and higher EF and FS (Figures 5J and 5L–5O). Also, gene expression of typical markers of hypertrophy (ANF, BNP) and fibrosis (Collagen

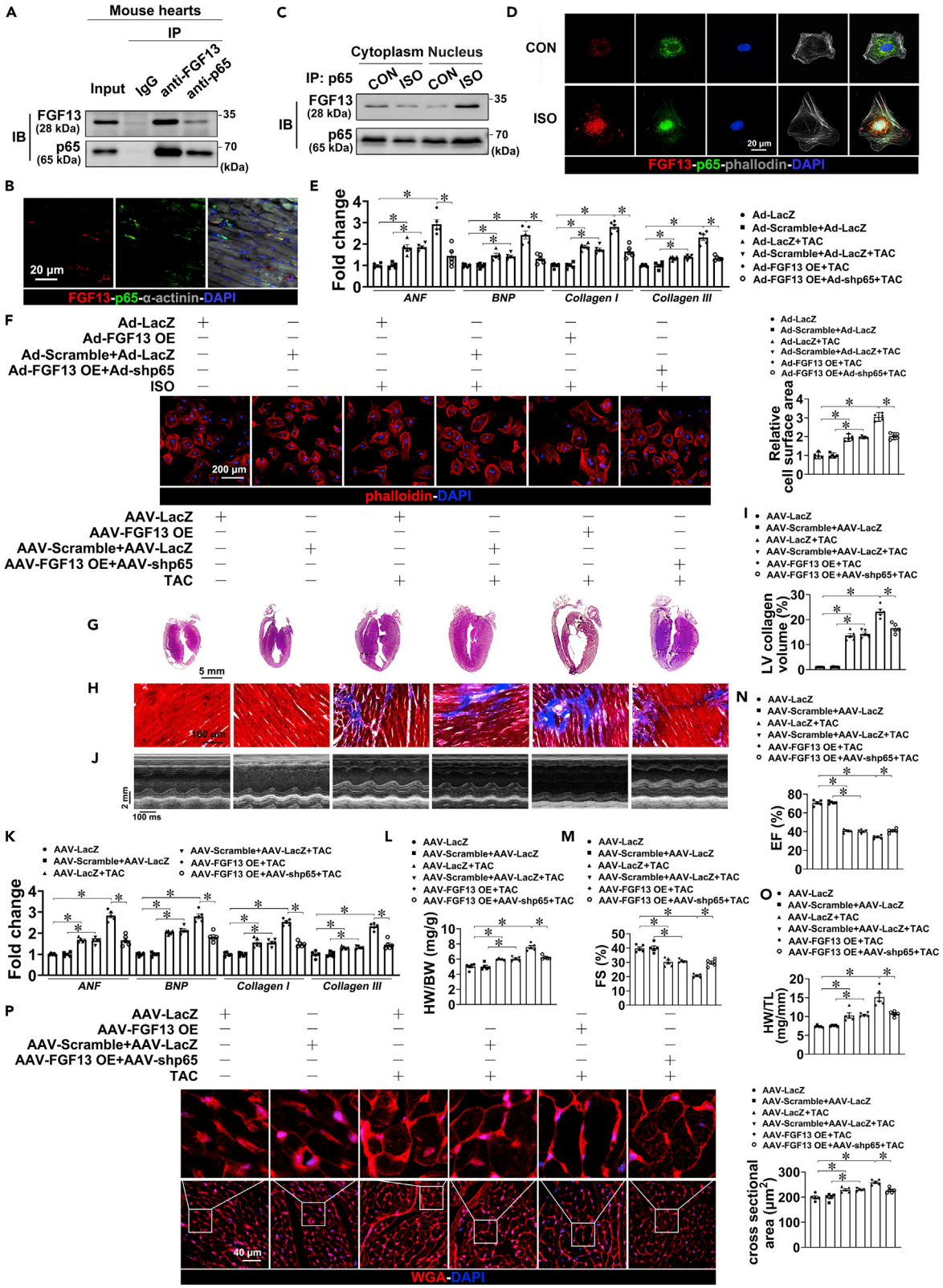
A
Mouse hearts
IP
Input
IgG
anti-FGF13
anti-p65
IB
FGF13 (28 kDa)
p65 (65 kDa)
35
70
(kDa)
C
Cytoplasm Nucleus
IP: p65
CON
ISO
CON
ISO
IB
FGF13 (28 kDa)
p65 (65 kDa)
35
70
(kDa)
D
CON
ISO
20 μm
FGF13-p65-phallodin-DAPI
B
20 μm
FGF13-p65-α-actinin-DAPI
E
Fold change
ANF
BNP
Collagen I
Collagen III
Ad-LacZ
Ad-Scramble+Ad-LacZ
Ad-LacZ+TAC
Ad-Scramble+Ad-LacZ+TAC
Ad-FGF13 OE+TAC
Ad-FGF13 OE+Ad-shp65+TAC
F
Ad-LacZ
Ad-FGF13 OE
Ad-Scramble+Ad-LacZ
Ad-FGF13 OE+Ad-shp65
ISO
TAC
200 μm
phalloidin-DAPI
Relative cell surface area
AAV-LacZ
AAV-FGF13 OE
AAV-Scramble+AAV-LacZ
AAV-FGF13 OE+AAV-shp65
G
5 mm
H
100 μm
I
LV collagen volume (%)
J
2 mm
100 ms
K
Fold change
ANF
BNP
Collagen I
Collagen III
L
HW/BW (mg/g)
M
FS (%)
N
EF (%)
O
HW/TL (mg/mm)
P
40 μm
WGA-DAPI
cross sectional area (μm²)

**Figure 5. The Central Roles of FGF13-p65 Interaction in Regulating Cardiac Hypertrophy**

(A) Immunoprecipitation with anti-FGF13 or anti-p65 from normal mouse hearts. The presence of co-precipitated endogenous p65 and FGF13 was determined by western blot. Inputs represent 1/10 of the lysates (n = 5 per group).

(B) IF staining for FGF13 (red) counterstained with p65 (green) on normal mouse hearts (n = 5 per group).

(C) Cytoplasm and nuclear extracts prepared from NRCMs, untreated or treated with ISO, were, respectively, precipitated with anti-p65 antibody. Co-precipitated FGF13 was detected by western blot (n = 5 per group).

(D) IF staining for FGF13 (red) counterstained with p65 (green) on NRCMs (n = 5 per group).

(E) qRT-PCR analysis of the *ANF, BNP, collagen I, collagen III* in NRCMs (n = 5 per group).

(F) Representative images of Phalloidin (red) and DAPI (blue)-stained NRCMs (n = 5 per group).

(G) Sagittal sections of mouse hearts stained with H&E (n = 5 per group).

(H) Heart sections stained with Masson (n = 5 per group).

(I) Quantification of the LV collagen volume in (H).

(J) Representative echocardiograms (n = 5 per group).

(K) qRT-PCR analysis of the *ANF, BNP, collagen I, collagen III, IL-6, IL-1β* in mouse hearts (n = 5 per group).

(L) Postmortem measurements of HW/BW (mg/g) (n = 5 per group).

(M and N) Measurement of EF (%) and FS (%) (n = 5 per group).

(O) Postmortem measurements of HW/TL (mg/mm) (n = 5 per group).

(P) IF staining for WGA (red) in mouse hearts (n = 5 per group).

Data are presented as mean ± SEM. *p < 0.05 represents statistically significant differences.

I, Collagen III) showed the similar trend (Figure 5K). These findings confirmed the central roles of FGF13-p65 interaction in the modulation of ISO- or TAC surgery-induced cardiomyocyte hypertrophy both *in vitro* and *in vivo*.

## NLS of FGF13 Is Necessary for NF-κB Activation during Cardiac Hypertrophy

We next sought to investigate the potential domain of FGF13 responsible for the interaction with p65. To obtain this, we made a series of FLAG-tagged deletion mutants of FGF13 (Figures S7A and S7 B). The pull-down assay with FLAG antibody showed that the 63–245 amino acid residues (63–245 aa) of FGF13 could not bind to p65, whereas the 1–62 aa, which contains the NLS, directly interacted with p65 (Figure 6A), suggesting that the NLS of FGF13 is indispensable for its interaction with p65.

To illustrate the functional importance of FGF13 NLS in regulating cardiac hypertrophy, an adenovirus expressing the FGF13 mutant form lacking the NLS (Ad-FGF13 NLS-) was generated to infect NRCMs (Figures S7C–S7E). Compared with the NRCMs infected with adenovirus-mediated full-length FGF13 overexpression (Ad-FGF13 WT), NRCMs infected with Ad-FGF13 NLS- lost the ability to further increase the activation of NF-κB under pressure overload. In detail, after ISO treatment, NRCMs infected with Ad-FGF13 NLS- showed similar nuclear p65 enrichment and the mRNA level of inflammatory genes (IL-6, IL-1β), along with analogous NF-κB luciferase activity, and IL-6, IL-1β protein levels to the NRCMs infected with Ad-LacZ (Figures 6B–6D and S7F). These data suggested that the NLS of FGF13 is crucial for the regulation of NF-κB. Also, the pro-hypertrophic effects of Ad-FGF13 WT were not observed in the FGF13 NLS- NRCMs (Figures 6C and 6E), which further confirmed the necessity of the FGF13 NLS in regulating NF-κB and modulating cardiac hypertrophy *in vitro*. Additionally, we explored whether nuclear enrichment of FGF13 is driven by p65. Western blotting analysis showed that the enhanced nuclear localization of FGF13 triggered by ISO was partially prevented by deficiency of p65 (Figure S7G), suggesting that p65 participates in FGF13 nuclear localization under pressure overload.

To verify the results observed *in vitro*, accordingly, we generated cardiac-specific FGF13 NLS- mice using AAV9-FGF13 NLS- by myocardial injection (Figures S7H and S7I), which were then exposed to TAC-surgery for 4 weeks. As expected, overexpression of FGF13 NLS- exerted no effects on the activation of NF-κB, as demonstrated by similar p65 nuclear localization (Figure 6F); the protein levels of IL-6, IL-1β; and the transcript levels of several NF-κB p65-targeted inflammation genes to single TAC-surgery mice (Figures 6G and S7J). Also, our results confirmed that, unlike the aggravated TAC-induced hypertrophic pathologies in the FGF13 WT mice, the extent of cardiac hypertrophy and fibrosis in the FGF13 NLS- mice was similar to that in the TAC mice (Figures 6H–6P).

## FGF13 OE Directly Induces NF-κB Activation in Cardiomyocytes under Basal Conditions

Considering the pivotal role of FGF13 in modulating NF-κB during cardiac hypertrophy, we finally discussed the role of FGF13 in NF-κB activation under basal conditions in cardiomyocytes. Without ISO

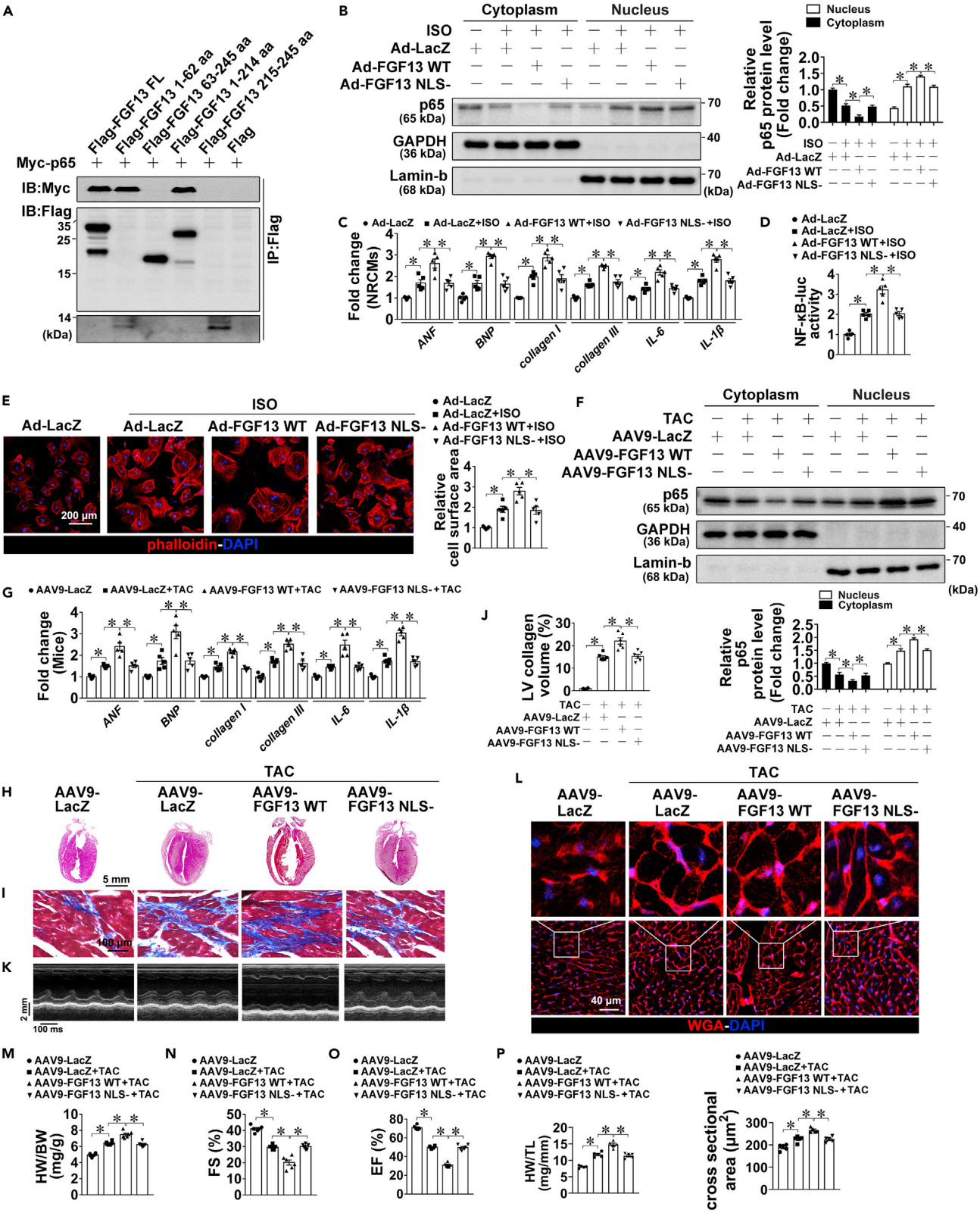
A
Flag-FGF13 FL
Flag-FGF13 1-62 aa
Flag-FGF13 63-245 aa
Flag-FGF13 1-214 aa
Flag-FGF13 215-245 aa
Flag
Myc-p65
IB:Myc
IB:Flag
IP:Flag
(kDa)
B
Cytoplasm
Nucleus
ISO
Ad-LacZ
Ad-FGF13 WT
Ad-FGF13 NLS-
p65 (65 kDa)
GAPDH (36 kDa)
Lamin-b (68 kDa)
Relative p65 protein level (Fold change)
C
Ad-LacZ
Ad-LacZ+ISO
Ad-FGF13 WT+ISO
Ad-FGF13 NLS-+ISO
Fold change (NRCMs)
ANF
BNP
collagen I
collagen III
IL-6
IL-1β
D
NF-κB-luc activity
E
Ad-LacZ
ISO
Ad-FGF13 WT
Ad-FGF13 NLS-
200 μm
phalloidin-DAPI
Relative cell surface area
F
TAC
AAV9-LacZ
AAV9-FGF13 WT
AAV9-FGF13 NLS-
G
AAV9-LacZ
AAV9-LacZ+TAC
AAV9-FGF13 WT+TAC
AAV9-FGF13 NLS-+TAC
Fold change (Mice)
J
LV collagen volume (%)
H
5 mm
I
100 μm
K
2 mm
100 ms
L
40 μm
WGA-DAPI
M
HW/BW (mg/g)
N
FS (%)
O
EF (%)
P
HW/TL (mg/mm)
cross sectional area (μm²)

**Figure 6. NLS of FGF13 Is Necessary for NF-κB Activation during Cardiac Hypertrophy**

(A) Immunoblotting was performed with indicated antibodies, following co-immunoprecipitation of the full-length and truncated mutants of FGF13 from HEK 293T whole-cell lysates using a FLAG antibody (n = 5 per group).
(B) Western blot analysis and quantification of p65 in cytoplasmic and nuclear extracts prepared from NRCMs (n = 5 per group).
(C) qRT-PCR analysis of the hypertrophic marker genes (*ANF*, *BNP*), fibrotic marker genes (*collagen I*, *collagen III*), and NF-κB targeted proinflammatory genes (*IL-6*, *IL-1β*) (n = 5 per group).
(D) NF-κB luciferase reporter assay (n = 5 per group).
(E) Representative images of Phalloidin (red) and DAPI (blue)-stained NRCMs (n = 5 per group).
(F) Western blot analysis and quantification of p65 in cytoplasmic and nuclear extracts prepared from mouse hearts (n = 5 per group).
(G) qRT-PCR analysis of the *ANF*, *BNP, collagen I, collagen III, IL-6, IL-1β* (n = 5 per group).
(H) Sagittal sections of mouse hearts stained with H&E (n = 6 per group).
(I) Heart sections stained with Masson (n = 6 per group).
(J) Quantification of the LV collagen volume in (I).
(K) Representative echocardiograms in mouse hearts (n = 6 per group).
(L) IF staining for WGA (red) in mouse hearts (n = 5 per group).
(M) Postmortem measurements of HW/BW (mg/g) (n = 6 per group).
(N and O) Measurement of EF (%) and FS (%) (n = 6 per group).
(P) Postmortem measurements of HW/TL (mg/mm) (n = 5 per group).
Data are presented as mean ± SEM. *p < 0.05 represents statistically significant differences.

stimulation, FGF13 OE alone was enough to promote NF-κB luciferase activity (Figure 7A) and p65 nuclear translocation (Figure 7B), thus facilitating the recruitment of the NF-κB p65-targeted inflammatory genes (Figures 7C and S6A) in NRCMs. Besides, although the mRNA levels of hypertrophic marker genes and fibrotic genes were increased by FGF13 OE (Figure 7C), it brought no effect on the morphological change in NRCMs (Figure 7D). The role of FGF13 in modulating NF-κB activation under basal conditions was also confirmed *in vivo*. Compared with the normal mice, the heart structure or function in FGF13 downregulated or overexpressed mice did not exhibit obvious abnormalities (Figures 7E–7N). However, FGF13-overexpressed mouse hearts showed the elevated NF-κB activation (Figures 7O and 7P), along with the elevated mRNA expression of hypertrophic marker genes and fibrotic genes (Figure 7O).

We also investigated whether NLS of FGF13 is necessary for NF-κB activation under basal conditions. Similar to the Ad-FGF13 WT treated NRCMs, FGF13 NLS- showed no apparent morphological change in NRCMs (Figure 7D). Also, FGF13 NLS- failed to activate NF-κB or increase the mRNA expression of hypertrophic marker genes as well as fibrotic genes compared with the FGF13 WT NRCMs (Figures 7A–7C and S8A). Consistent results were achieved *in vivo* (Figures 7E–7N and S8B). The effects of FGF13 in regulating NF-κB under basal conditions were independent of the phosphorylation or degradation of IκB (Figure S9) as well. Hence, the NLS of FGF13 is indispensable for FGF13 OE-induced NF-κB activation under basal conditions.

To further evaluate the involvement of FGF13 in regulating NF-κB activation under basal conditions, we infected NRCMs with Ad-p65 OE in the presence or absence of Ad-shFGF13. The results suggested that p65 OE enlarged the cell surface area, as well as increased hypertrophic marker genes (*ANF*, *BNP*), fibrotic markers (*Collagen I*, *Collagen III*), and inflammatory genes (*IL-6*, *IL-1β*) under basal conditions. Notably, the FGF13 deficiency reversed the effects of p65 OE. As expected, FGF13 downregulation reversed the increased NF-κB p65-targeted inflammatory genes expression induced by p65 OE (Figure S10), which robustly verified the critical involvement of FGF13 in NF-κB activation.

Considering that FGF13 OE alone was sufficient to activate NF-κB and to dramatically increase the mRNA levels of hypertrophic factors in mice, we asked whether prolonged FGF13 OE was sufficient to induce cardiac hypertrophy in mice. However, the hypertrophic phenotypes were not observed (Figure S11) even after the prolonged FGF13 OE for 20 weeks.

## DISCUSSION

NF-κB activity has been widely linked to normal biological processes and several human diseases (Gordon et al., 2011). Reports have showed that NF-κB activity is intricately controlled most notably through binding IκB proteins that tether NF-κB p65 in the cytoplasm until nuclear translocation is induced by signal-initiated IκB degradation (Hayden and Ghosh, 2004). In this study, an IκB-independent mechanism for NF-κB regulation in cardiomyocytes both under basal and stressful conditions has been revealed. Unlike IκB proteins that sequester p65 in the cytoplasm, FGF13-p65 complex formed under basal conditions and translocated

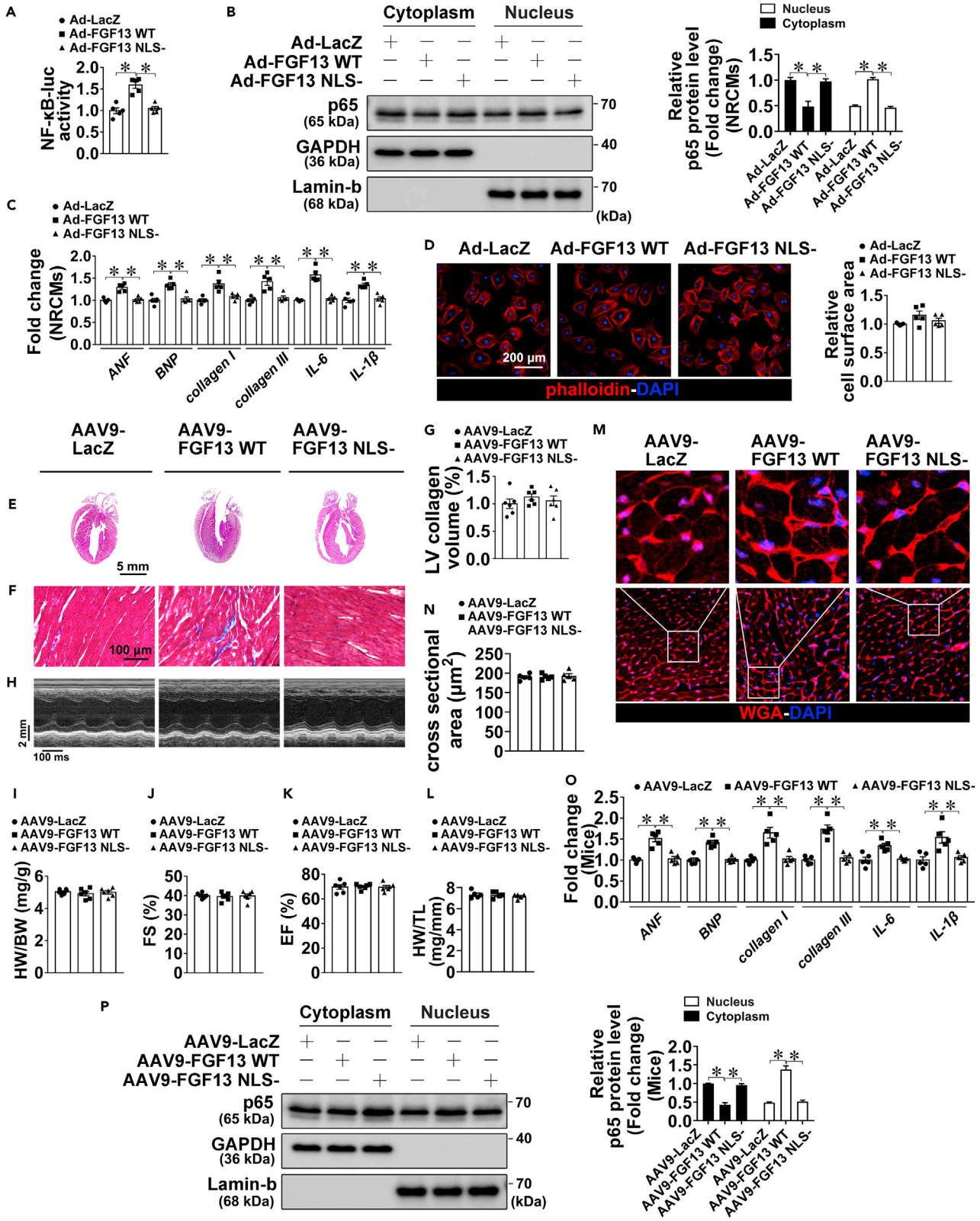
A
Ad-LacZ
Ad-FGF13 WT
Ad-FGF13 NLS-
NF-κB-luc activity
B
Cytoplasm
Nucleus
Ad-LacZ
Ad-FGF13 WT
Ad-FGF13 NLS-
p65 (65 kDa)
GAPDH (36 kDa)
Lamin-b (68 kDa)
(kDa)
Nucleus
Cytoplasm
Relative p65 protein level (Fold change) (NRCMs)
C
Fold change (NRCMs)
ANF
BNP
collagen I
collagen III
IL-6
IL-1β
D
Ad-LacZ
Ad-FGF13 WT
Ad-FGF13 NLS-
200 μm
phalloidin-DAPI
Relative cell surface area
AAV9-LacZ
AAV9-FGF13 WT
AAV9-FGF13 NLS-
E
5 mm
F
100 μm
H
2 mm
100 ms
G
LV collagen volume (%)
M
WGA-DAPI
N
cross sectional area (μm2)
I
HW/BW (mg/g)
J
FS (%)
K
EF (%)
L
HW/TL (mg/mm)
O
Fold change (Mice)
P
Relative p65 protein level (Fold change) (Mice)

**Figure 7. NLS of FGF13 Is Necessary for NF-κB Activation under Basal Conditions**

(A) NF-κB luciferase reporter assay (n = 5 per group).
(B) Western blot analysis and quantification of p65 in cytoplasmic and nuclear extracts (n = 5 per group).
(C) qRT-PCR analysis of *ANF*, *BNP*, *collagen I*, *collagen III*, *IL-6*, *IL-1β* (n = 5 per group).
(D) Representative images of Phalloidin (red) and DAPI (blue)-stained NRCMs (n = 5 per group).
(E) Sagittal sections of mouse hearts stained with H&E (n = 6 per group).
(F) Heart sections stained with Masson (n = 6 per group).
(G) Quantification of the LV collagen volume in (F).
(H) Representative echocardiograms (n = 6 per group).
(I) Postmortem measurements of HW/BW (mg/g) (n = 6 per group).
(J and K) Measurement of EF (%) and FS (%) (n = 6 per group).
(L) Postmortem measurements of HW/TL (mg/mm) (n = 5 per group).
(M) IF staining for WGA (red) in mouse hearts (n = 5 per group).
(N) Quantification of the cross-sectional area in (M).
(O) qRT-PCR analysis of the *ANF, BNP, collagen I, collagen III, IL-6, IL-1β* in mouse hearts (n = 5 per group).
(P) Western blot analysis and quantification of p65 in cytoplasmic and nuclear extracts (n = 5 per group).
Data are presented as mean ± SEM. *p < 0.05 represents statistically significant differences.

to the nucleus in response to cardiac hypertrophy. Furthermore, the NLS of FGF13 is necessary for its interaction with p65 and indispensable for its regulatory effect on pathological cardiac hypertrophy, indicating the prospective application of FGF13 as a therapeutic target for cardiomyopathies. Meanwhile, manipulation of FGF13 may be a novel strategy for NF-κB regulation.

FGF13 is the ancestral gene of the FGF family (Itoh and Ornitz, 2008). Although listed as a member of the FGF superfamily, FGF13 does not function as growth factors and is incapable of activating FGF receptors (Olsen et al., 2003). Rather, FGF13, as an intracellular protein, has been mostly extensively studied in regulating the electrical excitability of neurons (Schoorlemmer and Goldfarb, 2002; Itoh and Ornitz, 2008). In the heart, FGF13 was previously reported to regulate $Na^+$ channels, $Ca^{2+}$ channels, and their conduction. Also, FGF13 dictates myocardial excitability and affects arrhythmia susceptibility (Wang et al., 2011; Hennessey et al., 2013; Park et al., 2016; Wang et al., 2017). Recently, FGF13 has been shown to functionally interact with caveolin in the pathological remodeling of the heart with a hypertrophic phenotype (Wei et al., 2017). Nevertheless, the role of FGF13 in heart diseases has heretofore received less attention. Here we demonstrated that the expression of FGF13 was predominantly increased in ISO-treated NRCMs and TAC surgery-induced hypertrophic mouse hearts, accompanied by an increase in its nuclear localization. In particular, compared with the TAC-surgery mice, the FGF13 overexpressed mice with TAC-surgery for 4 weeks showed a decrease in EF and FS by at least 30%, indicating a state of heart failure. These results suggested that FGF13 plays a deleterious role in hypertrophic mouse hearts.

Although the main source of cytokines in the heart is the cardiac fibroblast (Porter and Turner, 2009), cardiomyocytes contribute to the inflammatory reaction (Yamauchi-Takihara et al., 1995; Song et al., 2010; Chelko et al., 2019). Hence, controlling the chain reaction of inflammation that occurs in resident cardiac cells, including cardiomyocytes, by inhibiting proinflammatory cytokine secretion can prevent cardiac damage during LV remodeling in an animal model (Aoyagi and Matsui, 2011). Some studies have demonstrated that targeting proinflammatory cytokine production specifically in cardiomyocytes might be a safer and more straightforward strategy in regression of hypertrophy/heart failure (van Empel and De Windt, 2004; Suckau et al., 2009; Liu et al., 2012). In this study, we investigated the signaling pathways responsible for FGF13-regulated pressure-overload-induced cardiac hypertrophy and found that NF-κB activation during cardiac hypertrophy process was effectively blocked by FGF13 deficiency in cardiomyocytes. In particular, FGF13 OE alone was sufficient to activate NF-κB in cardiomyocytes, which further illustrated the crucial role of FGF13 in hearts.

Hypertrophic hearts exhibit chronic activation of NF-κB and up-regulation of NF-κB-responsive genes. Although NF-κB has been considered as a pro-survival transcription factor, studies suggested that NF-κB activation can promote both survival and death pathways within the heart. Indeed, NF-κB can up-regulate both anti-apoptotic genes (TRAF1/2, cIAP-1/2, A1/Bfl-1, Bcl-XL, and cFLIP) and pro-apoptotic genes (Fas, FasL, DR4, DR5, DR6, TRAIL, and p53). In contrast, one other group has confirmed that the absence of p65-NF-κB conferred protection from deleterious remodeling, including decreased cardiomyocyte hypertrophy, heart mass, and fibrosis with preservation of contractile function (Liu et al., 2012). Strategies aimed at inhibiting NF-κB activity in the face of ischemia-reperfusion can protect the injured heart (Moss

et al., 2007; Stansfield et al., 2007; Hamid et al., 2011). Moreover, some evidence supports a cardioprotective role of NF-κB in models of coronary ligation and ischemic preconditioning (Tranter et al., 2010; Wilhide et al., 2011). As such, understanding the adaptive and maladaptive balance of NF-κB activation remains a largely unanswered question. In our study, we found that FGF13 ablation reduced pressure overload-induced NF-κB activation and cell death, along with decreased NF-κB targeted genes expression. On the contrary, FGF13 overexpression promoted the process of cardiac hypertrophy leading to heart failure. These findings support the idea that chronic activation of NF-κB signaling results in a prolonged inflammatory state thus leading to increased apoptotic cell death and progression toward heart failure (Gordon et al., 2011; Hamid et al., 2011). Therefore, targeting FGF13 in cardiomyocytes might be a therapeutic target for pathological cardiac hypertrophy and heart failure.

Canonically, NF-κB activation is triggered by phosphorylation-dependent degradation of the IκB proteins. Once in the nucleus, NF-κB p65 binds to κB response elements and initiates transcription (Purcell et al., 2001; Gilmore, 2006; Xing et al., 2006). Innovatively, we demonstrated FGF13 as a novel regulator of NF-κB directly binds to p65 through its NLS. Consistent with this idea, global protein-protein docking experiments and SPR assay confirmed the molecular interaction between FGF13 and p65. By contrast, FGF13 exhibited no effect on the phosphorylation or phosphorylation-induced degradation of IκB-α in NRCMs under basal or stressful conditions, indicating that FGF13 triggered the activation of NF-κB in an IκB-α-independent manner in NRCMs. As a family member of FHFs, FGF12 has been reported to interact with NEMO, an NF-κB essential modulator, to regulate NF-κB signaling in neurons (König et al., 2012). This provides further support that the interaction between p65 and FGF13 that we observed is functionally relevant.

It is interesting to note that FGF13 has dual roles in organism. On a positive note, the FGF13 gene is located on the chromosome Xq26 segment and is important in embryonic development (Smallwood et al., 1996; Gecz et al., 1999). FGF13$^{-/-}$ mice are embryonic lethal at day E10.5 and exhibit large pericardial effusion (Puranam et al., 2015). Meanwhile, FGF13 acts as a microtubule-stabilizing protein and regulates the function of NaVs in neurons (Wu et al., 2012). Under hypertrophic conditions, FGF13 can protect the heart against conduction failure via regulating myocardial excitability (Park et al., 2016). As an unfavorable factor, however, FGF13 knockout in adult hearts not only increases the density of caveolae but also enhances mechanoprotection of cardiomyocytes in the setting of increased ventricular loading (Wei et al., 2017). Here, we revealed that FGF13 is an unfavorable factor in pathological myocardial hypertrophy under pressure overload. Moreover, FGF13 OE alone does not bring on cardiac hypertrophy but promotes the NF-κB activity and leads to increased expression of NF-κB p65-dependent genes. This may be attributed to the fact that the pathological hypertrophic response is coordinated by a complex hypertrophic network that comprises numerous signaling pathways (van Berlo et al., 2013; Heineke and Molkentin, 2016). Thus, it is hard to infer whether FGF13 is an unfavorable factor or not in cardiomyocytes and hearts under basal conditions.

In summary, our findings demonstrate that FGF13 is a potent regulator of NF-κB activity in cardiomyocytes both in basal and stimulated conditions and the NLS of FGF13 is necessary in the process. Moreover, these results further extend the repertoire of the known modulatory effects of FGF13 beyond ion channel regulation. It will be of interest to extend the role of FGF13-p65 interaction in some other cardiomyopathies.

## Limitation of the Study

This study did not investigate whether signaling derived by the upregulated FGF13 in cardiomyocytes can affected non-myocytes under pressure overload. Our experimental evidence suggests that FGF13 deficiency in cardiomyocytes has a global protective role during cardiac hypertrophy. However, at present, we lack information on the mechanism of this cross talk. Further investigation is required into the possible roles that FGF13 may play in cardiomyocytes—non-myocytes communications during cardiac hypertrophy.

## Resource Availability

### *Lead Contact*

Further information and requests for resources and reagents should be directed to and will be fulfilled by the Lead Contact, Xiaokun Li (profxiaokunli@163.com).

### *Materials Availability*

New unique reagents were not generated in this study.

*Data and Code Availability*

The data in this study are available from the corresponding author on request.

## METHODS

All methods can be found in the accompanying Transparent Methods supplemental file.

## SUPPLEMENTAL INFORMATION

Supplemental Information can be found online at https://doi.org/10.1016/j.isci.2020.101627.

## ACKNOWLEDGMENTS

This work was supported by the National Natural Science Foundation of China under Grants (grant nos.81900240, 81800236, 81570368, 81600304, 81770498), the Natural Science Foundation of Zhejiang Province (grant nos. LYY18H310009, LQ18H020004), the Zhejiang Province Medical and Health Science Program (grant no. 2019RC054), and the Wenzhou Science and Technology Bureau Foundation (grant nos. Y20160004, Y20190164).

## AUTHOR CONTRIBUTIONS

J.S.: Conceptualization, Writing – original draft, Methodology, Figures, Writing – review & editing. C.N.: Funding acquisition, Conceptualization, Methodology, Study design. W.Y.: Funding acquisition, Figures, Data analysis. N.A.: Methodology, Writing – review & editing. G.C.: Methodology, Figures. X.H.: Funding acquisition, Methodology. J.W.: Methodology. X.C.: Methodology. Y.S.: Writing – review & editing. S.H.: Writing – review & editing. Ying Wang: Data analysis. X.W.: Funding acquisition, Data analysis. Yang Wang: Data analysis, Methodology. L.J.: Funding acquisition, Supervision, Data analysis, Writing –review & editing. W.C.: Funding acquisition, Supervision, Data analysis, Writing – review & editing. X.L.: Conceptualization, Supervision, Writing – original draft, Data analysis, Writing – review & editing.

## DECLARATION OF INTERESTS

The authors declare that they have no competing interests.

Received: December 19, 2019
Revised: August 13, 2020
Accepted: September 25, 2020
Published: October 23, 2020

## REFERENCES

Aoyagi, T., and Matsui, T. (2011). The cardiomyocyte as a source of cytokines in cardiac injury. J. Cell Sci. Ther. *2012*, 003.

Barnes, P.J., and Karin, M. (1997). Nuclear factor-kappa B: a pivotal transcription factor in chronic inflammatory diseases. New Engl. J. Med. *336*, 1066–1071.

Brown, K., Gerstberger, S., Carlson, L., Franzoso, G., and Siebenlist, U. (1995). Control of I kappa B-alpha proteolysis by site-specific, signal-induced phosphorylation. Science *267*, 1485–1488.

Chelko, S.P., Asimaki, A., Lowenthal, J., Bueno-Beti, C., Bedja, D., Scalco, A., Amat-Alarcon, N., Andersen, P., Judge, D.P., Tung, L., et al. (2019). Therapeutic modulation of the immune response in arrhythmogenic cardiomyopathy. Circulation *140*, 1491–1505.

DiDonato, J., Mercurio, F., Rosette, C., Wu-Li, J., Suyang, H., Ghosh, S., and Karin, M. (1996). Mapping of the inducible IkappaB phosphorylation sites that signal its ubiquitination and degradation. Mol. Cell Biol. *16*, 1295–1304.

Gecz, J., Baker, E., Donnelly, A., Ming, J.E., McDonald-McGinn, D.M., and Spinner, N.B. (1999). Fibroblast growth factor homologous factor 2 (FHF2): gene structure, expression and mapping to the Börjeson-Forssman-Lehmann syndrome region in Xq26 delineated by a duplication breakpoint in a BFLS-like patient. Hum. Genet. *104*, 56–63.

Ghosh, S., and Baltimore, D. (1990). Activation in vitro of NF-kappa B by phosphorylation of its inhibitor I kappa B. Nature *344*, 678–682.

Gilmore, T.D. (2006). Introduction to NF-kappaB: players, pathways, perspectives. Oncogene *25*, 6680–6684.

Goldfarb, M., Schoorlemmer, J., Williams, A., Diwakar, S., Wang, Q., Huang, X., Giza, J., Tchetchik, D., Kelley, K., Vega, A., et al. (2007). Fibroblast growth factor homologous factors control neuronal excitability through modulation of voltage-gated sodium channels. Neuron *55*, 449–463.

Gordon, J.W., Shaw, J.A., and Kirshenbaum, L.A. (2011). Multiple facets of NF-κB in the heart: to be or not to NF-κB. Circ. Res. *108*, 1122–1132.

Gupta, S., and Sen, S. (2005). Role of the NF-kappaB signaling cascade and NF-kappaB-targeted genes in failing human hearts. J. Mol. Med. (Berl) *83*, 993–1004.

Hall, G., Hasday, J.D., and Rogers, T.B. (2006). Regulating the regulator: NF-kappaB signaling in heart. J. Mol. Cell Cardiol *41*, 580–591.

Hamid, T., Guo, S.Z., Kingery, J.R., Xiang, X., Dawn, B., and Prabhu, S.D. (2011). Cardiomyocyte NF-κB p65 promotes adverse remodelling, apoptosis, and endoplasmic reticulum stress in heart failure. Cardiovasc. Res. *89*, 129–138.

Hayden, M.S., and Ghosh, S. (2004). Signaling to NF-kappaB. Genes Dev. *18*, 2195–2224.

Heineke, J., and Molkentin, J.D. (2006). Regulation of cardiac hypertrophy by intracellular signalling pathways. Nat. Rev. Mol. Cell Biol. *7*, 589–600.

Hennessey, J.A., Wei, E.Q., and Pitt, G.S. (2013). Fibroblast growth factor homologous factors modulate cardiac calcium channels. Circ. Res. *113*, 381–388.

Hsu, W.C., Nilsson, C.L., and Laezza, F. (2014). Role of the axonal initial segment in psychiatric disorders: function, dysfunction, and intervention. Front. Psychiatry *5*, 109.

Itoh, N., and Ornitz, D.M. (2008). Functional evolutionary history of the mouse Fgf gene family. Dev. Dyn. *237*, 18–27.

Jones, W.K., Brown, M., Wilhide, M., He, S., and Ren, X. (2005). NF-kappaB in cardiovascular disease: diverse and specific effects of a "general" transcription factor? Cardiovasc. Toxicol. *5*, 183–202.

Karin, M. (1999). How NF-kappaB is activated: the role of the IkappaB kinase (IKK) complex. Oncogene *18*, 6867–6874.

Konhilas, J.P., Watson, P.A., Maass, A., Boucek, D.M., Horn, T., Stauffer, B.L., Luckey, S.W., Rosenberg, P., and Leinwand, L.A. (2006). Exercise can prevent and reverse the severity of hypertrophic cardiomyopathy. Circ. Res. *98*, 540–548.

König, H.G., Fenner, B.J., Byrne, J.C., Schwamborn, R.F., Bernas, T., Jefferies, C.A., and Prehn, J.H. (2012). Fibroblast growth factor homologous factor 1 interacts with NEMO to regulate NF-κB signaling in neurons. J. Cell Sci. *125*, 6058–6070.

Kreusser, M.M., Lehmann, L.H., Keranov, S., Hoting, M.O., Oehl, U., Kohlhaas, M., Reil, J.C., Neumann, K., Schneider, M.D., Hill, J.A., et al. (2014). Cardiac CaM Kinase II genes δ and γ contribute to adverse remodeling but redundantly inhibit calcineurin-induced myocardial hypertrophy. Circulation *130*, 1262–1273.

Levy, D., Kenchaiah, S., Larson, M.G., Benjamin, E.J., Kupka, M.J., Ho, K.K., Murabito, J.M., and Vasan, R.S. (2002). Long-term trends in the incidence of and survival with heart failure. N. Engl. J. Med. *347*, 1397–1402.

Liu, Q., Chen, Y., Auger-Messier, M., and Molkentin, J.D. (2012). Interaction between NFκB and NFAT coordinates cardiac hypertrophy and pathological remodeling. Circ. Res. *110*, 1077–1086.

Molkentin, J.D., Lu, J.R., Antos, C.L., Markham, B., Richardson, J., Robbins, J., Grant, S.R., and Olson, E.N. (1998). A calcineurin-dependent transcriptional pathway for cardiac hypertrophy. Cell *93*, 215–228.

Moss, N.C., Stansfield, W.E., Willis, M.S., Tang, R.H., and Selzman, C.H. (2007). IKKbeta inhibition attenuates myocardial injury and dysfunction following acute ischemia-reperfusion injury. Am J Physiol Heart Circ Physiol *293*, H2248–H2253.

Olsen, S.K., Garbi, M., Zampieri, N., Eliseenkova, A.V., Ornitz, D.M., Goldfarb, M., and Mohammadi, M. (2003). Fibroblast growth factor (FGF) homologous factors share structural but not functional homology with FGFs. J. Biol. Chem. *278*, 34226–34236.

Park, D.S., Shekhar, A., Marra, C., Lin, X., Vasquez, C., Solinas, S., Kelley, K., Morley, G., Goldfarb, M., and Fishman, G.I. (2016). Fhf2 gene deletion causes temperature-sensitive cardiac conduction failure. Nat. Commun. *7*, 12966.

Porter, K.E., and Turner, N.A. (2009). Cardiac fibroblasts: at the heart of myocardial remodeling. Pharmacol. Ther. *123*, 255–278.

Puranam, R.S., He, X.P., Yao, L., Le, T., Jang, W., Rehder, C.W., Lewis, D.V., and McNamara, J.O. (2015). Disruption of Fgf13 causes synaptic excitatory-inhibitory imbalance and genetic epilepsy and febrile seizures plus. J. Neurosci. *35*, 8866–8881.

Purcell, N.H., Tang, G., Yu, C., Mercurio, F., DiDonato, J.A., and Lin, A. (2001). Activation of NF-kappa B is required for hypertrophic growth of primary rat neonatal ventricular cardiomyocytes. Proc. Natl. Acad. Sci. U S A *98*, 6668–6673.

Schoorlemmer, J., and Goldfarb, M. (2002). Fibroblast growth factor homologous factors and the islet brain-2 scaffold protein regulate activation of a stress-activated protein kinase. J. Biol. Chem. *277*, 49111–49119.

Simpson, P. (1985). Stimulation of hypertrophy of cultured neonatal rat heart cells through an alpha 1-adrenergic receptor and induction of beating through an alpha 1- and beta 1-adrenergic receptor interaction. Evidence for independent regulation of growth and beating. Circ. Res. *56*, 884–894.

Smallwood, P.M., Munoz-Sanjuan, I., Tong, P., Macke, J.P., Hendry, S.H., Gilbert, D.J., Copeland, N.G., Jenkins, N.A., and Nathans, J. (1996). Fibroblast growth factor (FGF) homologous factors: new members of the FGF family implicated in nervous system development. Proc. Natl. Acad. Sci. U S A *93*, 9850–9857.

Song, X., Kusakari, Y., Xiao, C.Y., Kinsella, S.D., Rosenberg, M.A., Scherrer-Crosbie, M., Hara, K., Rosenzweig, A., and Matsui, T. (2010). mTOR attenuates the inflammatory response in cardiomyocytes and prevents cardiac dysfunction in pathological hypertrophy. Am. J. Physiol. Cell Physiol. *299*, C1256–C1266.

Stansfield, W.E., Moss, N.C., Willis, M.S., Tang, R., and Selzman, C.H. (2007). Proteasome inhibition attenuates infarct size and preserves cardiac function in a murine model of myocardial ischemia-reperfusion injury. Ann Thorac Surg *84*, 120–125.

Suckau, L., Fechner, H., Chemaly, E., Krohn, S., Hadri, L., Kockskämper, J., Westermann, D., Bisping, E., Ly, H., Wang, X., et al. (2009). Long-term cardiac-targeted RNA interference for the treatment of heart failure restores cardiac function and reduces pathological hypertrophy. Circulation *119*, 1241–1252.

Tranter, M., Ren, X., Forde, T., Wilhide, M.E., Chen, J., Sartor, M.A., Medvedovic, M., and Jones, W.K. (2010). NF-kappaB driven cardioprotective gene programs; Hsp70.3 and cardioprotection after late ischemic preconditioning. J Mol Cell Cardiol *49*, 664–672.

Ucar, A., Gupta, S.K., Fiedler, J., Erikci, E., Kardasinski, M., Batkai, S., Dangwal, S., Kumarswamy, R., Bang, C., Holzmann, A., et al. (2012). The miRNA-212/132 family regulates both cardiac hypertrophy and cardiomyocyte autophagy. Nat. Commun. *3*, 1078.

Valen, G. (2004). Signal transduction through nuclear factor kappa B in ischemia-reperfusion and heart failure. Basic Res. Cardiol. *99*, 1–7.

Van, Berlo, J.H., Maillet, M., and Molkentin, J.D. (2013). Signaling effectors underlying pathologic growth and remodeling of the heart. J. Clin. Invest. *123*, 37–45.

Van, Empel, V.P., and De, Windt, L.J. (2004). Myocyte hypertrophy and apoptosis: a balancing act. Cardiovasc. Res. *63*, 487–499.

Wang, C., Hennessey, J.A., Kirkton, R.D., Wang, C., Graham, V., Puranam, R.S., Rosenberg, P.B., Bursac, N., and Pitt, G.S. (2011). Fibroblast growth factor homologous factor 13 regulates $Na^+$ channels and conduction velocity in murine hearts. Circ. Res. *109*, 775–782.

Wang, X., Tang, H., Wei, E.Q., Wang, Z., Yang, J., Yang, R., Wang, S., Zhang, Y., Pitt, G.S., Zhang, H., and Wang, C. (2017). Conditional knockout of Fgf13 in murine hearts increases arrhythmia susceptibility and reveals novel ion channel modulatory roles. J. Mol. Cell Cardiol. *104*, 63–74.

Wei, E.Q., Sinden, D.S., Mao, L., Zhang, H., Wang, C., and Pitt, G.S. (2017). Inducible Fgf13 ablation enhances caveolae-mediated cardioprotection during cardiac pressure overload. Proc. Natl. Acad. Sci. U S A *114*, E4010–E4019.

Wilhide, M.E., Tranter, M., Ren, X., Chen, J., Sartor, M.A., Medvedovic, M., and Jones, W.K. (2011). Identification of a NF-κB cardioprotective gene program: NF-κB regulation of Hsp70.1 contributes to cardioprotection after permanent coronary occlusion. J Mol Cell Cardiol *51*, 82–89.

Wu, Q.F., Yang, L., Li, S., Wang, Q., Yuan, X.B., Gao, X., Bao, L., and Zhang, X. (2012). Fibroblast growth factor 13 is a microtubule-stabilizing protein regulating neuronal polarization and migration. Cell *149*, 1549–1564.

Xiao, M., Bosch, M.K., Nerbonne, J.M., and Ornitz, D.M. (2013). FGF14 localization and organization of the axon initial segment. Mol. Cell Neurosci *56*, 393–403.

Xing, W., Zhang, T.C., Cao, D., Wang, Z., Antos, C.L., Li, S., Wang, Y., Olson, E.N., and Wang, D.Z. (2006). Myocardin induces cardiomyocyte hypertrophy. Circ. Res. *98*, 1089–1097.

Yamauchi-Takihara, K., Ihara, Y., Ogata, A., Yoshizaki, K., Azuma, J., and Kishimoto, T. (1995). Hypoxic stress induces cardiac myocyte-derived interleukin-6. Circulation *91*, 1520–1524.

**iScience, Volume *23***

## Supplemental Information

# FGF13 Is a Novel Regulator of NF-κB and Potentiates Pathological Cardiac Hypertrophy

**Jia Sun, Chao Niu, Weijian Ye, Ning An, Gen Chen, Xiaozhong Huang, Jianan Wang, Xixi Chen, Yingjie Shen, Shuai Huang, Ying Wang, Xu Wang, Yang Wang, Litai Jin, Weitao Cong, and Xiaokun Li**

## Supplemental Information

## Supplemental Figures

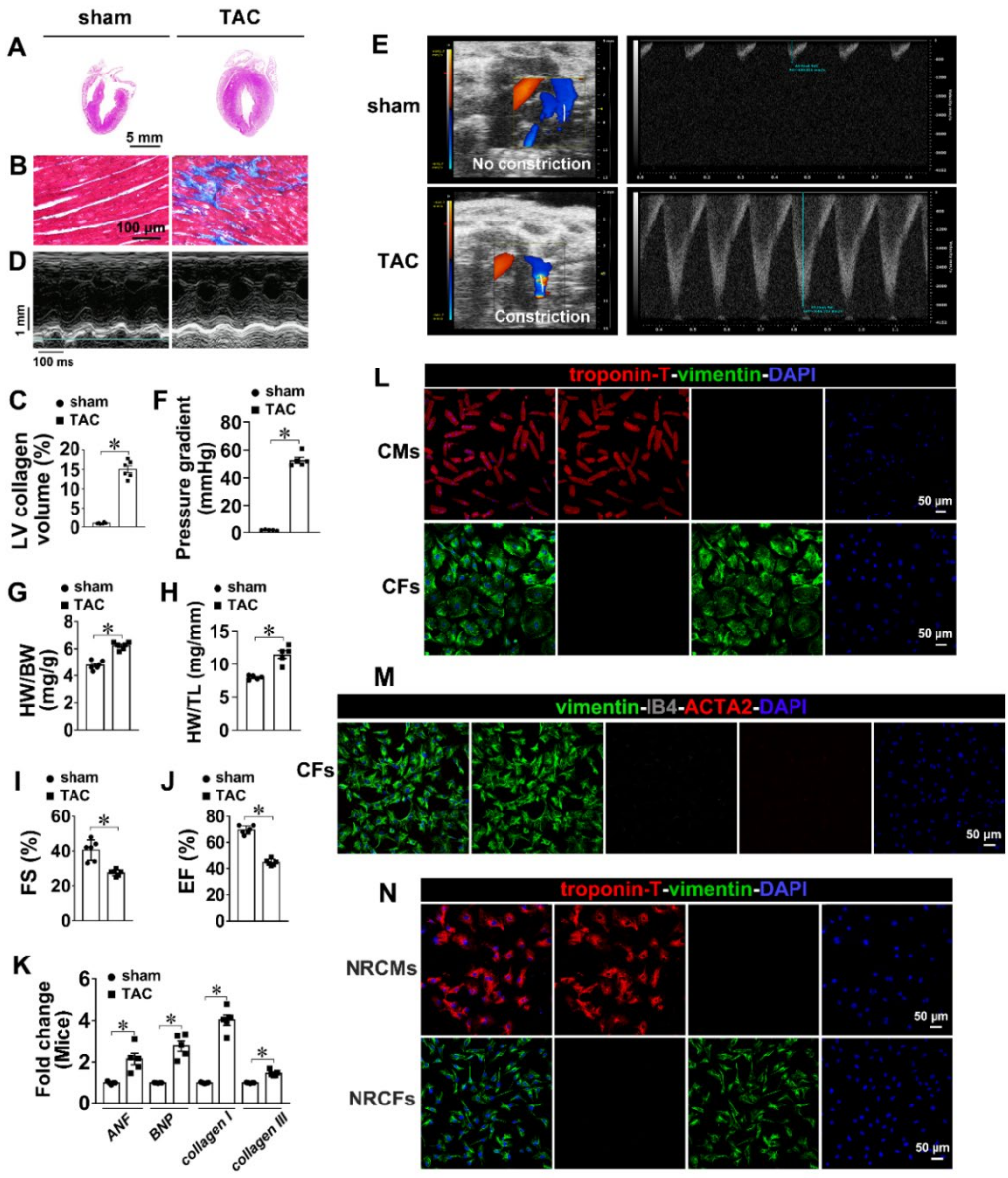


**Figure S1:** Endogenous FGF13 is up-regulated in TAC-surgery mice (4 weeks) in cardiomyocytes. Related to Figure 1. (A) Sagittal sections of sham and TAC-surgery mouse hearts stained with H&E (n=6 per group). (B) Heart sections stained with Masson (n=6 per group). (C) Comparison of the LV collagen volume in the indicated groups. (D) Representative echocardiograms from sham and TAC surgery mouse hearts (n=6 per group). (E) Color and PW Doppler images from sham and TAC hearts are shown (n=5 per group). (F) Peak aortic velocity obtained from PW Doppler imaging is used to calculate pressure gradient according to the modified Bernoulli's equation (pressure gradient = 4 x $V_{max}^2$). (G) Postmortem measurements of HW/BW

(mg/g) (n=6 per group). (H) Postmortem measurements of HW/TL (mg/mm) (n=5 per group). (I, J) Measurement of EF (%) and FS (%) (n=6 per group). (K) qPCR analysis of the hypertrophic marker genes (*ANF*, *BNP*), fibrotic marker genes (*collagen I*, *collagen III*) from the sham and TAC surgery mouse hearts (n=5 per group). (L) IF staining of isolated CMs and CFs from mouse hearts with cardiac troponin-T antibody (red), vimentin antibody (green), and DAPI. (M) IF staining of isolated CFs from mouse hearts with vimentin antibody, Isolectin-B4 antibody, ACTA2 antibody, and DAPI. (N) IF staining of isolated NRCMs and NRCFs from 1- to 2-day-old SD rat pups with cardiac troponin-T antibody (red), vimentin antibody (green), and DAPI. Data are presented as mean ± SEM. *$p < 0.05$ represents statistically significant differences.

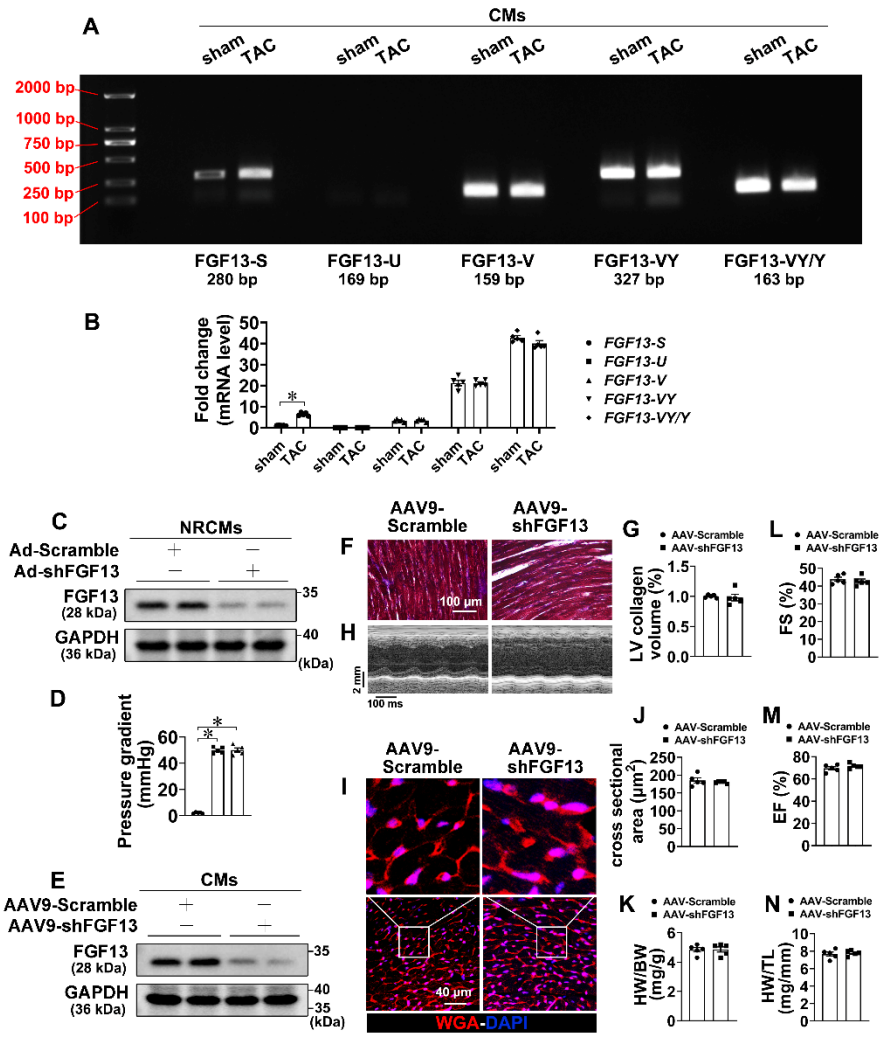


**Figure S2:** FGF13-S mRNA level was significantly higher in hypertrophic CMs, and FGF13 deficiency at baseline showed no significant differences in heart phenotype or cardiac function. Related to Figure 1; Figure 2. (A) sqRT-PCR analysis of FGF13 in CMs (n=5 per group). (B) qRT-PCR analysis of FGF13 in CMs (n=5 per group). (C) FGF13 knockdown in NRCMs validated by western blotting (n=5 per group). (D) Peak aortic velocity obtained from PW Doppler imaging is used to calculate pressure gradient according to the modified Bernoulli's equation. (E) FGF13 knockdown in CMs isolated from mouse hearts (n=5 per group). (F) Heart sections stained with Masson (n=5 per group). (G) Comparison of the LV collagen volume in the indicated groups. (H) Representative echocardiograms (n=5 per group). (I) IF staining for WGA (red) in mouse hearts (n=5 per group). (J) Quantification of the cross sectional area in (F). (K) Postmortem measurements of HW/BW (mg/g) (n=5 per group). (L, M) Measurement of FS (%) and EF (%) (n=5 per group). (N) Postmortem measurements of HW/TL (mg/mm) (n=5 per group). Data are presented as mean ± SEM. *p < 0.05 represents statistically significant differences.

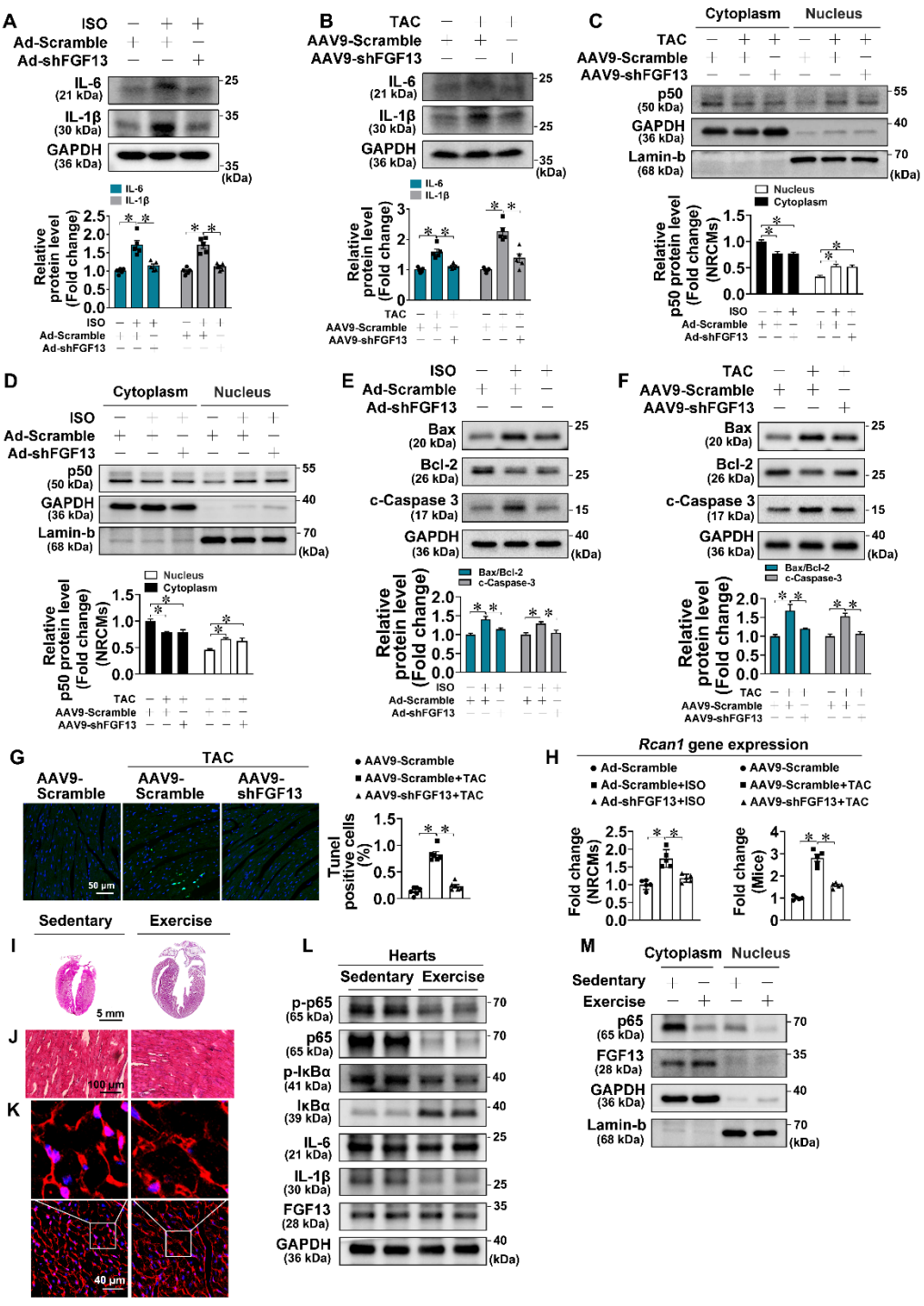


**Figure S3:** Inhibition targeting of FGF13 ameliorated the detrimental effects of pressure overload. Related to Figure 2. (A) Immunoblots and quantification of the expression levels of IL-6 and IL-1β in NRCMs (n=5 per group). (B) Immunoblots and quantification of the expression levels of IL-6 and IL-1β in mouse hearts (n=5 per group). (C) Western blot analysis and quantification of p50 in cytoplasmic and nuclear extracts prepared in NRCMs (n=5 per group). (D) Western blot analysis of p50 in cytoplasmic and nuclear extracts prepared in mouse hearts (n=5 per group). (E)

Immunoblots and quantification of the expression levels of Bax/Bcl-2 and c-Caspase 3 in NRCMs (n=5 per group). (F) Immunoblots and quantification of the expression levels of Bax/Bcl-2 and c-Caspase 3 in mouse hearts (n=5 per group). (G) Representative confocal images and quantification of Tunel positive cells in heart sections. (H) qRT-PCR analysis of Rcan1 in NRCMs and mouse hearts (n=5 per group). (I) Sagittal sections of mouse hearts stained with H&E (n=5 per group). (J) Heart sections stained with Masson (n=5 per group). (K) Immunofluorescence staining for WGA (red) in mouse hearts (n=5 per group). (L) Immunoblots of the expression levels of p-p65, p65, p-IκBα, IκBα, IL-6, IL-1β and FGF13 in hearts (n=5 per group). (M) Western blot analysis of p65 and FGF13 in cytoplasmic and nuclear extracts prepared in hearts (n=5 per group). Data are presented as mean ± SEM. *$p < 0.05$ represents statistically significant differences.

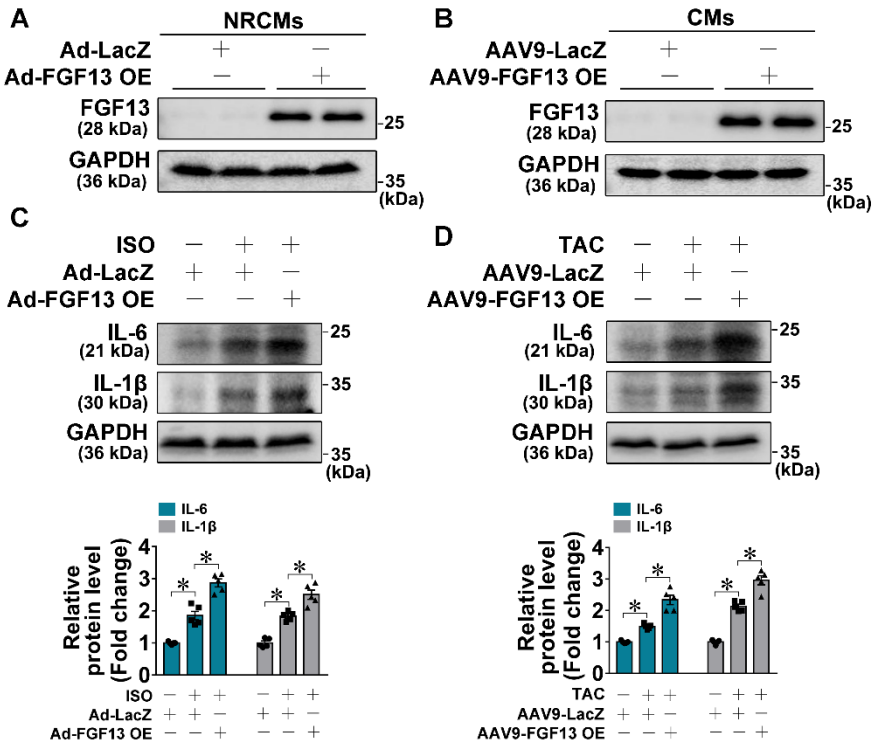


**Figure S4:** Forced FGF13 OE exacerbated pathological cardiac hypertrophy. Related to Figure 3. (A) FGF13 OE in NRCMs validated by western blotting (n=5 per group). (B) FGF13 overexpression in CMs isolated from mouse hearts (n=5 per group). (C) Immunoblots and quantification of the expression levels of IL-6 and IL-1β in NRCMs (n=5 per group). (D) Immunoblots and quantification of the expression levels of IL-6 and IL-1β in mouse hearts (n=5 per group). Data are presented as mean ± SEM. *p < 0.05 represents statistically significant differences.

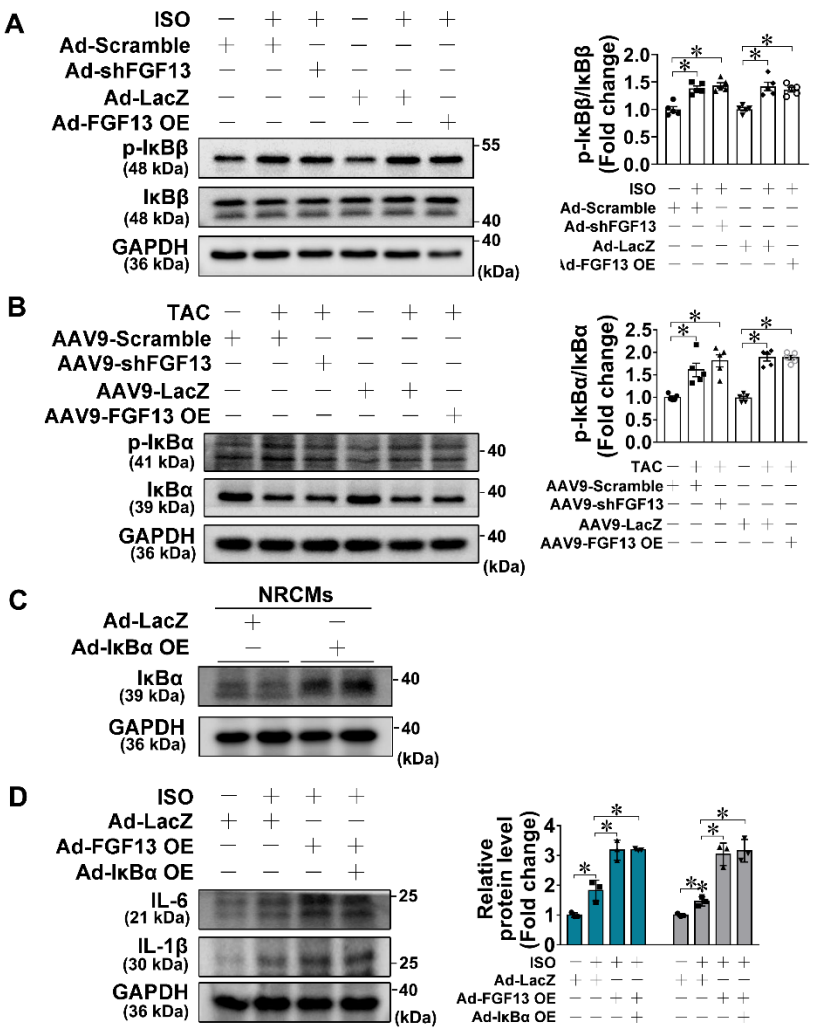


**Figure S5:** FGF13 regulates NF-κB activation in response to pressure overload via an IκB-independent manner. Related to Figure 4. (A) Immunoblots and quantification of the expression levels of p-IκBβ and IκBβ in NRCMs (n=5 per group). (B) Immunoblots and quantification of the expression levels of p-IκBα and IκBα in mouse hearts (n=5 per group). (C) IκBα OE in NRCMs validated by western blotting (n=5 per group). (D) Immunoblots and quantification of the expression levels of IL-6 and IL-1β in NRCMs (n=5 per group). Data are presented as mean ± SEM. *p < 0.05 represents statistically significant differences.

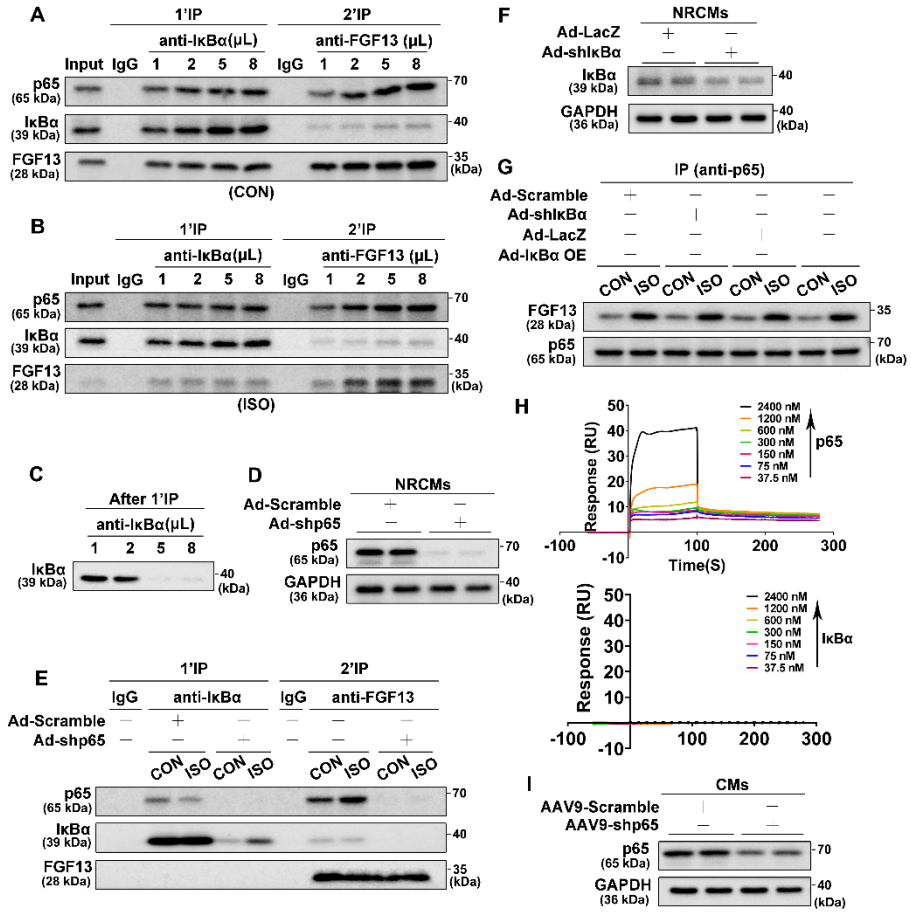


**Figure S6:** FGF13 interacts with p65. Related to Figure 5. Proteins (p65, IκBα, FGF13) detected in lysates (n=5 per group). Whole cell lysates of NRCMs (A) or ISO-treated cell lysates (B) were initially immunoprecipitated with the indicated amounts of anti-IκBα antibodies (463.3 μg/mL) or rabbit IgG as a control. Then the unbound fractions were reimmunoprecipitated with anti-FGF13 antibodies (200 μg/mL) or goat IgG as a control. Inputs represent 1/10 of the lysates. (C) Immunoblots of the expression level of IκBα in the unbound fractions. (D) p65 knockdown in NRCMs validated by western blotting (n=5 per group). (E) Proteins (p65, IκBα, FGF13) detected in lysates (n=5 per group). Cell lysates were precipitated with anti-IκBα antibody or rabbit IgG as a control. The unbound fractions were reimmunoprecipitated with anti-FGF13 antibody or goat IgG as a control. Inputs represent 1/10 of the lysates. (F) IκBα knockdown in NRCMs validated by western blotting (n=5 per group). (G) Proteins (p65, FGF13) detected in lysates immunodepleted of IκBα (n=5 per group). Whole cell lysates of NRCMs were immunoprecipitated with the indicated amounts of anti-IκBα antibodies. (H) Representative graphs from surface plasmon resonance spectroscopy analysis (n=5 per group). (I) p65 knockdown in CMs isolated from mouse hearts (n=5 per group).

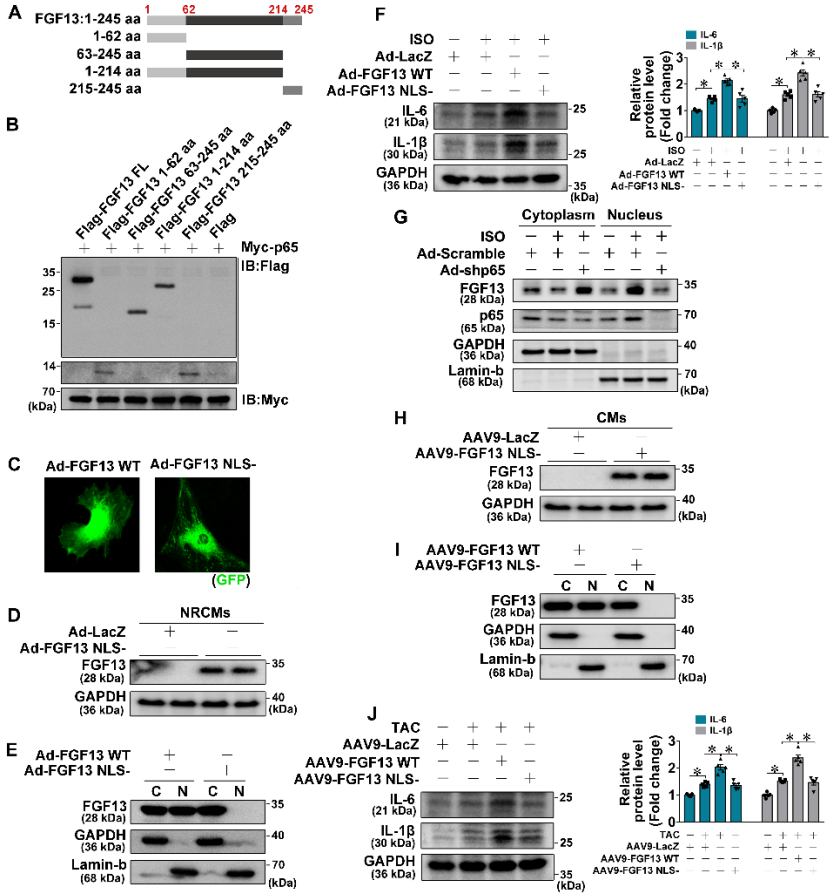


**Figure S7:** NLS of FGF13 is necessary for NF-κB activation under pressure overload. Related to Figure 6. (A) Schematic of the full-length and truncated mutants of FGF13. (B) Western blot of the truncated mutants of FGF13 from HEK 293T whole-cell lysates (n=5 per group). (C) Localization of the GFP-FGF13 WT and GFP-FGF13 NLS- fusion proteins in NRCMs were analyzed by confocal microscopy (n=5 per group). (D) Immunoblots of the expression levels of FGF13 in NRCMs (n=5 per group). (E) Localization of the GFP-FGF13 WT and GFP-FGF13 NLS- fusion proteins in NRCMs were analyzed by immunoblotting (n=5 per group). (F) Immunoblots and quantification of the expression levels of IL-6 and IL-1β in NRCMs (n=5 per group). (G) Western blot analysis of endogenous FGF13 and p65 in cytoplasmic and nuclear extracts prepared from NRCMs (n=5 per group). (H) Immunoblots of the expression levels of FGF13 in CMs isolated from mouse hearts. (I) Immunoblots of the localization of the GFP-FGF13 WT and GFP-FGF13 NLS- fusion proteins in CMs isolated from mouse hearts. (n=5 per group). (J) Immunoblots and quantification of the expression levels of IL-6 and IL-1β in mouse hearts (n=5 per group). Data are presented as mean ± SEM. *p < 0.05 represents statistically significant differences.

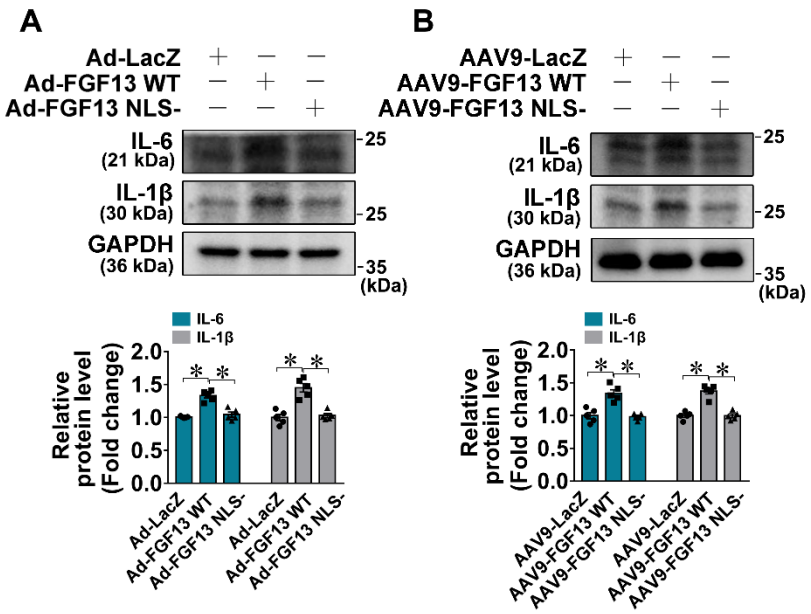


**Figure S8:** NLS of FGF13 is necessary for NF-κB activation under basal conditions. Related to Figure 7. (A) Immunoblots and quantification of the expression levels of IL-6 and IL-1β in NRCMs (n=5 per group). (B) Immunoblots and quantification of the expression levels of IL-6 and IL-1β in mouse hearts (n=5 per group). Data are presented as mean ± SEM. *p < 0.05 represents statistically significant differences.

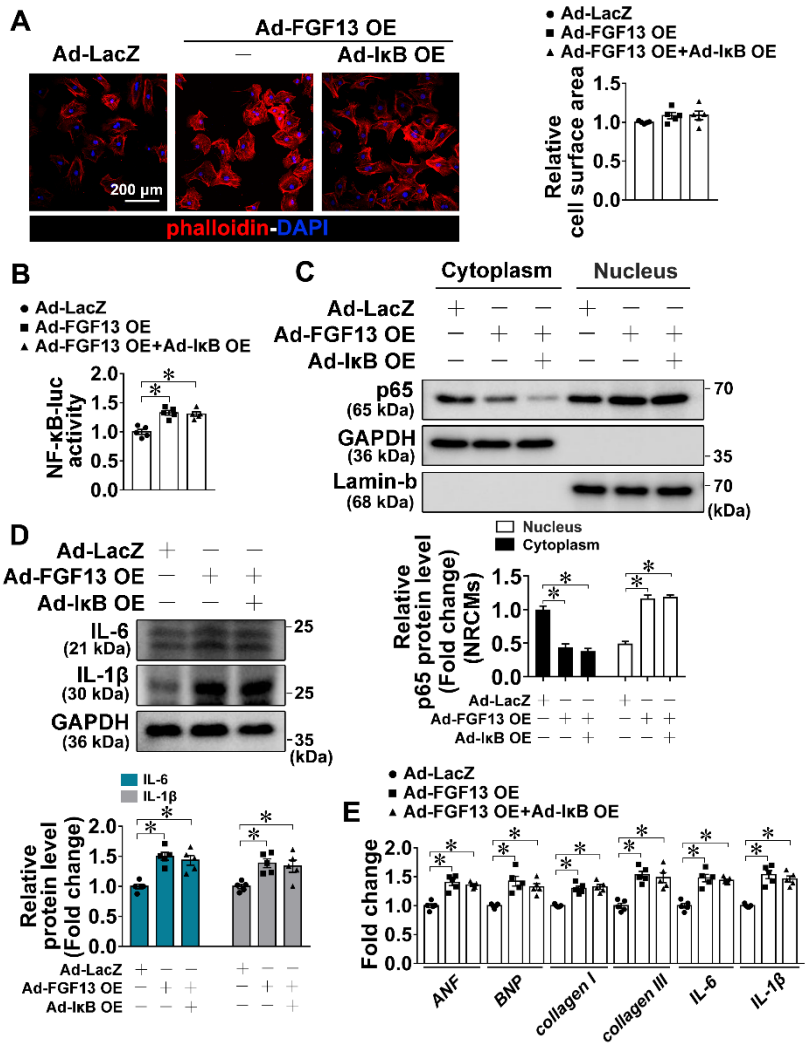


143

144 **Figure S9:** The effects of FGF13 in regulating NF-κB under basal conditions were
145 independent of the phosphorylation or degradation of IκB. Related to Figure 7. (A)
146 Representative images of Phalloidin (red) and DAPI (blue) stained NRCMs (n=5 per
147 group). (B) NF-κB-luciferase activity in NRCMs (n=5 per group). (C) Western blot
148 analysis and quantification of endogenous p65 in cytoplasmic and nuclear extracts
149 (n=5 per group). (D) Immunoblots and quantification of the expression levels of IL-6
150 and IL-1β (n=5 per group). (E) qPCR analysis of the hypertrophic marker genes (*ANF*,
151 *BNP*), fibrotic marker genes (*collagen I*, *collagen III*) and NF-κB targeted
152 proinflammatory genes (*IL-6*, *IL-1β*) in NRCMs (n=5 per group). Data are presented
153 as mean ± SEM. *p < 0.05 represents statistically significant differences.

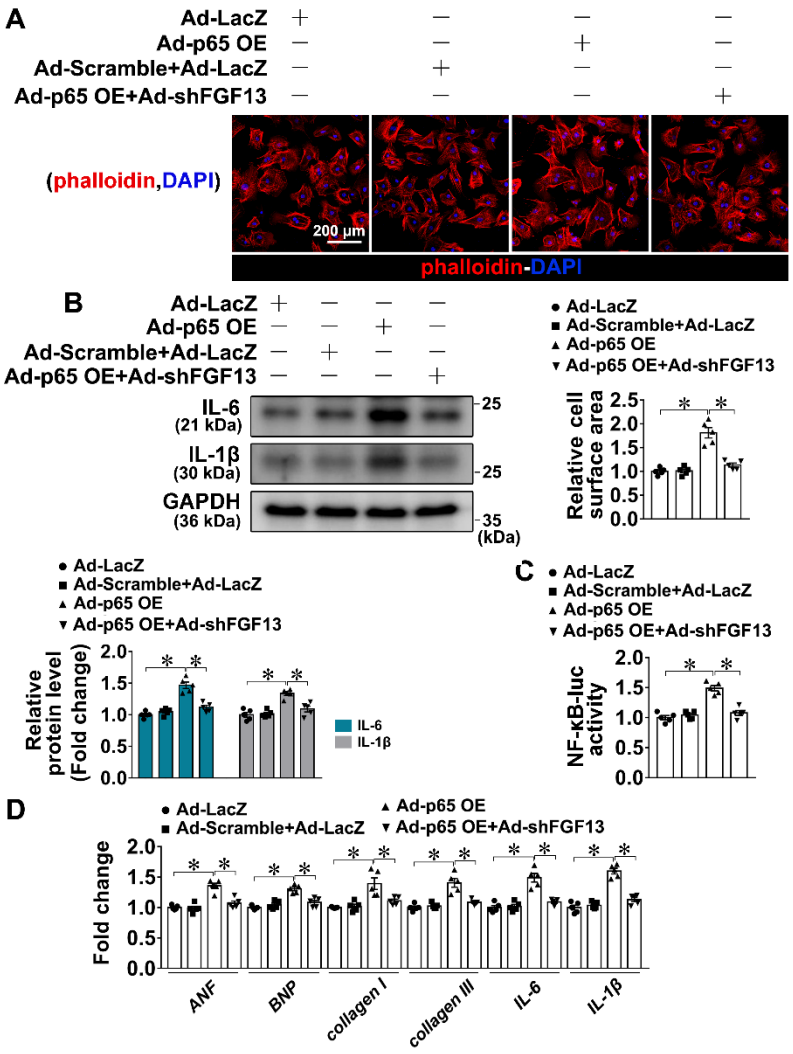


**Figure S10:** FGF13 is indispensable for regulating NF-κB activation under basal conditions. Related to Figure 7. (A) Representative images of Phalloidin (red) and DAPI (blue) stained NRCMs (n=5 per group). (B) Immunoblots and quantification of the expression levels of IL-6 and IL-1β (n=5 per group). (C) NF-κB-luciferase activity in NRCMs (A) (n=5 per group). (D) qPCR analysis of the hypertrophic marker genes (*ANF*, *BNP*), fibrotic marker genes (*collagen I*, *collagen III*) and NF-κB targeted proinflammatory genes (*IL-6*, *IL-1β*) in NRCMs (n=5 per group). Data are presented as mean ± SEM. *p < 0.05 represents statistically significant differences.

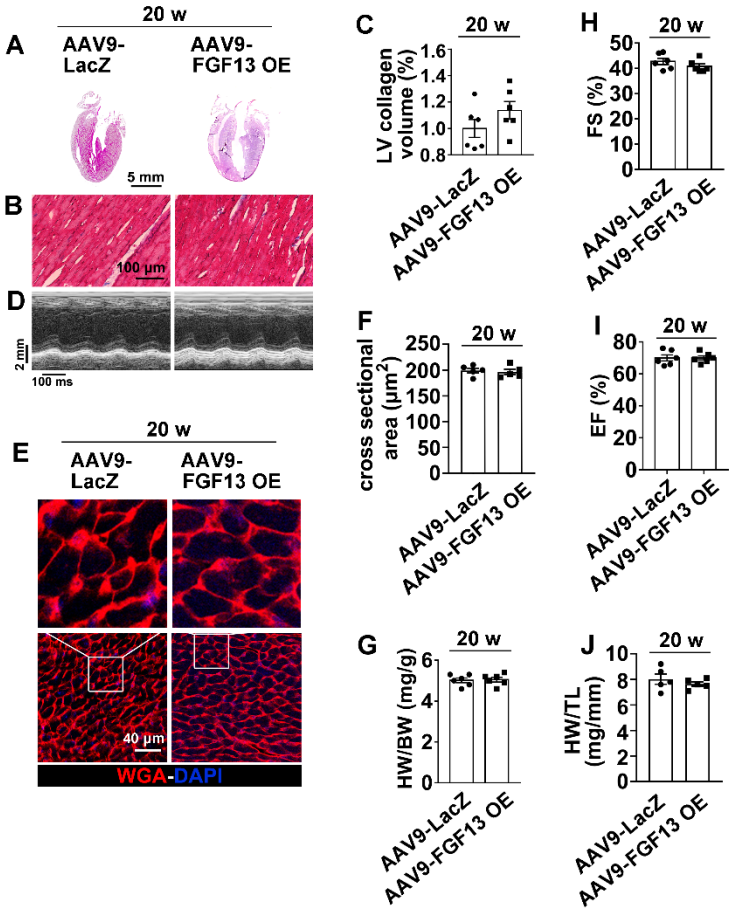


**Figure S11:** Prolonged FGF13 OE for 20 weeks in mouse hearts does not cause hypertrophic phenotypes. Related to Figure 7. (A) Sagittal sections of mouse hearts stained with H&E (n=6 per group). (B) Heart sections stained with Masson (n=6 per group). (C) Comparison of the LV collagen volume in the indicated groups. (D) Representative echocardiograms (n=6 per group). (E) Immunofluorescence staining for WGA (red) in mouse hearts (n=5 per group). (F) Quantification of the cross sectional area in (E). (G) Postmortem measurements of HW/BW (mg/g) (n=6 per group). (H, I) Measurement of FS (%) and EF (%) (n=6 per group). (J) Postmortem measurements of HW/TL (mg/mm) (n=5 per group).

## Transparent Methods

### Animals studies

All animal procedures confirmed to the guidelines from Directive 2010/63/EU of the European Parliament on the protection of animals used for scientific purposes, and all animal experiments involving animals were approved by the Animal Care and Use Committee of Wenzhou Medical University, China (wydw2019-0837). 6-8 weeks old male C57BL/6J mice weighing 22-30 g were obtained from Model Animal Research Center of Nanjing University and housed in a temperature-controlled room under a 12 h/12 h-light/dark and allowed access to tap water ad libitum. Mice were sacrificed with an overdose of sodium pentobarbital (200 mg/kg, ip) at the end of experiments.

### Exercise-induced model of physiological cardiac hypertrophy-swim training

Physiological hypertrophy in mice was achieved via swim training twice daily for 4 weeks, as previously described (McMullen et al., 2003). Swim training commenced in adult mice at approximately 3 months of age with 10 min sessions on the first day, with 10 min increments each day until the maximum of 90 min per session was reached. Mice were rested for at least 4 h between each session, and water temperature was maintained between 30℃ and 32℃ to avoid thermal stress. At the end of every session, mice were individually towel dried to prevent hypothermia. Hearts were collected 3 h after the last swim session.

### Adeno-associated virus 9 (AAV9) delivery

AAV9 harboring FGF13 shRNA (AAV9-shFGF13), FGF13 overexpression vector (AAV9-FGF13 OE, also named as AAV9-FGF13 WT), and NLS deficient FGF13 overexpression vector (AAV9-FGF13 NLS-) were cloned into AAV9-EGFP plasmid under a MCMV promoter (entrusted by OBIO TECHNOLOGY (SHANGHAI) CORP), respectively. AAV9 harboring the Scramble (an in-house generated shRNA; AAV9-Scramble) or β-galactosidase (AAV9-LacZ) were used as the control. We used AAV9 because it shows strong tropism for the heart, particularly for cardiomyocytes, and yields long-term gene expression (Inagaki K et al., 2006; Pacak CA et al., 2006; Zincarelli C et al., 2008; Suckau L et al., 2009; Hulot JS et al., 2011). The virus was delivered into the heart by myocardial injection. Firstly, mice were placed in a supine position under a heating lamp and orally intubated to 2% isoflurane (RWD Life Science Co., Shenzhen, China) with a flow of 1.0 L/min and 100% $O_2$. The heart was exposed upon opening the left pleural cavity by cutting the left third and fourth ribs and intercostal muscles. The pericardium was removed, and a syringe fitted with a

29-G needle was intramuscularly inserted near the apex of the heart and the anterior left ventricle with 10 μL of AAV vector ($5 \times 10^{10}$ vg per point), respectively. Finally, the chest was closed in layers. Three-weeks later, they were subjected to TAC or sham surgery.

### *In vivo* cardiac hypertrophy

For induction of cardiac hypertrophy in mice, transverse aortic constriction (TAC) was performed as previously described (Rockman HA et al., 1991; Furihata T et al., 2016). The mouse was fixed in a supine position with the neck slightly extended. A 20-G catheter was inserted through the larynx into the trachea with care taken not to puncture the trachea or other structures in the pharyngeal region. Ventilation was performed with a tidal volume of 200 μL, respiratory rate of 120/min, 95% oxygen. Body temperature was maintained as close as possible to 37˚C throughout the experiment using a self-regulating heating pad. After disinfection with 2% iodine, the chest cavity was opened by an incision of the left second intercostal space. The aortic arch was dissected from the surrounding tissue. The pericardial sac was opened while a 6-0 suture was passed underneath the transverse aorta and ligated over a 27-G needle, which was removed later to provide a lumen. The chest cavity, muscle and skin were closed layer by layer. Sham-operated mice underwent similar surgical procedures, including isolation of the aorta and looping of the aorta, but without tying of the suture. Mice were observed until recovery in a 37˚C heated cage. Mice of different genotypes were randomly assigned to the sham or TAC groups.

All analyses were performed at 4 weeks post TAC unless otherwise specified.

### Echocardiographic assessment

Cardiac geometry and function were evaluated by echocardiography, using a high-resolution echocardiography machine. All measurements were averaged at least six consecutive cardiac cycles. Color and pulse wave (PW) Doppler imaging was used to noninvasively measure pressure gradient across the aortic constriction created by TAC and to assess transmitral blood flow in mice. Calculate pressure gradient across the constricted site using the modified Bernoulli's equation: pressure gradient = 4 x $V_{max}^2$. Only include mice with a pressure gradient ranging from 40 to 80 mmHg for further analysis.

### Histology

Mice were sacrificed with an overdose of sodium pentobarbital (200 mg/kg, ip) at the end of experiments. The mouse hearts were then fixed with 4% paraformaldehyde at

4˚C for 24 h, dehydrated with 20% sucrose and 30% sucrose, embedded in Tissue-Tek optimal cutting temperature compound (OCT, Sakura Finetek Inc) and finally snap frozen and stored at -80°C. For histological analysis, the specimens were cut into 10 μm cryostat sections, and mounted onto Superfrost Ultra Plus glass slides. Hematoxylin and eosin (H&E) and Masson's trichrome staining were performed according to routine procedures. Myocyte cross sectional areas were measured, using NIH Image J software (National Institutes of Health, Bethesda, MD, USA), in sections stained with fluorescein conjugated wheat germ agglutinin (WGA-Alexa Fluor 350, Invitrogen, Carlsbad, CA, USA). The fibrotic areas were measured using Image-Pro Plus software (version 6.0) with captured images. At least 100 randomly selected myocytes cut transversely were measured from three animals/group.

***In vivo* immunofluorescence staining**

Briefly, sections were permeabilized with 0.3% Triton X-100 for 30 min and blocked with 10% donkey serum at room temperature for 1 h. The slices were then co-incubated with anti-FGF13 antibody (sc16811; Santa Cruz Biotechnology, Santa Cruz, CA, USA) and anti-α-actinin antibody (1:100; 6487; Cell Signaling Technology, Danvers, MA, USA) at 4˚C overnight. Finally, sections were incubated with Alexa Flour 488-conjugated donkey anti-goat antibody (1:250; ab150129; Abcam, Cambridge, MA, USA) and Alexa Flour 647-conjugated donkey anti-rabbit antibody (1:250; ab150075; Abcam, Cambridge, MA, USA) at 4˚C overnight and nucleus were stained with 4,6 diamidino-2-phenylindole (DAPI) for 20 min. Sections were measured using Leica TCS SP5 Confocal microscope (Leica, Wetzlar, Germany). Data were confirmed by a blinded pathologist.

**Isolation, culture and adenoviral infection of neonatal rat cardiomyocytes (NRCMs)**

NRCMs were isolated according to previously described standard protocols (Vandergriff AC et al., 2015). 1- to 2-day-old SD rat pups were rinsed quickly in 70% ethanol solution for surface sterilization. Hearts were extracted from the body with curved scissors and transferred immediately into cold DPBS (14190144; Gibco BRL, Grand Island, NY, USA). The tissue was minced into small pieces (approximately 0.5-1 $mm^3$, or smaller), which were then transferred into a conical tube containing trypsin medium (0.08% trypsin (T8150; Shanghai Solarbio Bioscience & Technology Co., Shanghai, China), 0.8% NaCl (V900058; Sigma-Aldrich, St. Louis, MO, USA), 0.03% KCl (V900068; Sigma-Aldrich, St. Louis, MO, USA), 0.035% $NaHCO_3$ (V900182; Sigma-Aldrich, St. Louis, MO, USA), 0.1% D-(+)-Glucose (G7021;

Sigma-Aldrich, St. Louis, MO, USA) and 0.2% Hepes (H3375; Sigma-Aldrich, St. Louis, MO, USA)) with 37˚C water bath and magnetic stirring (100 rpm) for 8 min per time. Removing the digestion solution (cell suspension) and adding the fresh trypsin medium for further digestion until the tissue disappeared.

Gathering the digestion solution and filtering through sterile 200 m nylon and centrifuging at 1000 rpm for 3 minutes to pellet cells. The cells were resuspended in plating medium DMEM/F12 (11330032; Gibco BRL, Grand Island, NY, USA) supplemented with 10% fetal calf serum (16010159; Gibco BRL, Grand Island, NY, USA), 2% penicillin/streptomycin (P1400; Shanghai Solarbio Bioscience & Technology Co., Shanghai, China), plated into 10 $cm^2$ cell culture dish and incubated for 1-3 h in cell culture incubator to remove fibroblasts (NRCFs) and endothelial cells. The NRCFs were obtained from the adherent cells after 2 times of passages. After incubation, washing non-adherent NRCMs from 10 $cm^2$ culture dish and seeding at a density of $1.5\times10^5$ cells per well onto collagen (C919; Sigma-Aldrich, St. Louis, MO, USA) coated six-well culture plates, which consisted of DMEM/F12 supplemented with 10% fetal calf serum, 5-bromodeoxyuridine (0.1 mM, to inhibit fibroblast proliferation) (B5002; Sigma-Aldrich, St. Louis, MO, USA) and 1% penicillin/streptomycin.

Adenoviral vector harboring FGF13 shRNA (Ad-shFGF13), FGF13 (Ad-FGF13 OE, also named as Ad-FGF13 WT in Fig. 6, 7), and NLS deficient FGF13 overexpression (Ad-FGF13 NLS-) were cloned into pAdeno-EGFP plasmid under a MCMV promoter (entrusted by OBIO TECHNOLOGY (SHANGHAI) CORP), respectively. Adenoviruses harboring a scrambled sequence (Ad-scramble) or β-galactosidase (Ad-LacZ) were used as the control. For adenoviral infection (MOI=20), virus was resuspended in culture medium (serum free) and added to cells when they were switched from plating medium. Cells were checked with GFP fluorescence 24-48 h post infection for subsequent experiments. For the assessment of cardiomyocyte hypertrophy, NRCMs were subsequently stimulated with ISO (10 μM) for 48 h (Simpson P, 1985).

**Isolation of viable cardiac myocytes (CMs) and cardiac fibroblastes (CFs) from adult mouse hearts**

CMs and CFs were isolated according to previously described standard protocols (Ackers-Johnson M et al., 2016). Firstly, the mice were anesthetized and the chest was opened to expose the heart. Descending aorta was cut and the heart was immediately flushed by injection of 7 mL EDTA buffer (NaCl: 130 mM, KCl: 5 mM, $NaH_2PO_4$

(S8282; Sigma-Aldrich, St. Louis, MO, USA): 0.5 mM, Hepes: 10 mM, Glucose: 10 mM, BDM (B0753; Sigma-Aldrich, St. Louis, MO, USA): 10 mM, Taurine (T8691; Sigma-Aldrich, St. Louis, MO, USA): 10 mM, EDTA (EDS; Sigma-Aldrich, St. Louis, MO, USA): 5 mM) into the right ventricle. Ascending aorta was clamped using reynolds forceps and the heart was transferred to a dish containing fresh EDTA buffer. Digestion was achieved by sequential injection of 10 mL EDTA buffer, 3 mL perfusion buffer (NaCl: 130 mM, KCl: 5 mM, $NaH_2PO_4$: 0.5 mM, HEPEs: 10 mM, Glucose: 10 mM, BDM: 10 mM, Taurine: 10 mM, $MgCl_2$ (M8266; Sigma-Aldrich, St. Louis, MO, USA): 1 mM), and 30-50 mL collagenase buffer (collagenase 2 (LS004176; Worthington, USA): 0.5 mg/mL, collagenase 4 (LS004188; Worthington, USA): 0.5 mg/mL, protease XIV (P5147; Sigma-Aldrich, St. Louis, MO, USA): 0.05 mg/mL) into the left ventricle. Constituent chambers were then separated and gently pulled into 1 mm pieces using forceps. Cellular dissociation was completed by gentle trituration and enzyme activity was inhibited by addition of 5 mL stop buffer (perfusion buffer containing 5% sterile FBS). Cell suspension was passed through a 100 μm filter. The cell pellet ultimately formed a highly pure myocyte fraction. The CMs were re-suspended in pre-warmed plating media (M199 (M4530; Sigma-Aldrich, St. Louis, MO, USA): 93 mL/100 mL, FBS: 5%, BDM: 10 mM), and plated onto laminin (8 μg/mL; 23017-15; Gibco BRL, Grand Island, NY, USA) pre-coated tissue-culture plastic. After 1 h, and every 48 h thereafter, media was changed to fresh, pre-warmed culture media (M199: 96 mL/100 mL, BSA: 0.1%, ITS (I3146; Sigma-Aldrich, St. Louis, MO, USA): 1×, BDM: 10 mM, CD lipid (11905-031; Gibco BRL, Grand Island, NY, USA): 1×). Additionally, the supernatant was combined to produce a fraction containing CFs. The fractions were centrifuged (300 g, 5 min), re-suspended in fibroblast growth media (DMEM/F12: 90 mL/100 mL, FBS: 10%) and plated on tissue-culture treated plastic. Media was changed after 24 h every 48 h thereafter.

**Plasmid constructs**

DNA fragments that encoded the various FGF13-S (1-245 aa, 1-62 aa, 63-245 aa, 1-214 aa and 215-245 aa) and p65 (1-551 aa) truncates were cloned into the pcDNA3.1 (+)-Flag-C1 and pcDNA3.1 (+)-Myc-C1 expression vectors, respectively (entrusted by OBIO TECHNOLOGY (SHANGHAI) CORP).

**Surface plasmon resonance (SPR) analysis**

Sensor grams were recorded on a Biacore 3000 instrument. Briefly, recombinant human FGF13 protein (NBP2-35009; NOVUS Biologicals, Littleton, CO, USA) was

immobilized on the research grade CM5 sensor chip in 10 mM sodium acetate (pH 5.5), using the manufacturer's amine coupling kit. Unreacted residues on the surface were blocked by two washes with 1 M ethanolamine (pH 8.5). Different concentrations of NF-κB p65 (12054-H09E-50; Sino Biological Inc., Beijing, China) (at 2400, 1200, 600, 300, 150, 75, 37.5 nM) or IκBα (12045-H07E; Sino Biological Inc., Beijing, China) (at 2400, 1200, 600, 300, 150, 75, 37.5 nM) were prepared with the running buffer (PBS, 0.1%SDS, 5%DMSO). Sensors and sample plate were placed on the instrument. The interactions were determined according to the manufacturer's instructions at a flow rate of 30 $\mu L \cdot min^{-1}$ for 120 s during the association phase followed by 120 s for the dissociation phase at 25˚C.

**HEK293T culture and transfection**

HEK293T cells were maintained in high glucose DMEM (10-013-CV; Cellgro, Herndon, VA) supplemented with 10% FBS, 1% penicillin and streptomycin. The cells were transfected with the constructed plasmids (Flag-FGF13 FL (full length), Flag-FGF13 1-62 aa, Flag-FGF13 63-245 aa, Flag-FGF13 1-214 aa, Flag-FGF13 215-245 aa, Myc-p65 FL, or pcDNA 3.1 empty vector (8 μg) with Lipofectamine 2000 (11668019; Invitrogen, Carlsbad, CA, USA) according to the manufacturer's protocol. At 48 h post transfection, western blot analysis was performed to confirm the efficiency of transfection.

***In vitro* immunofluorescence staining**

Briefly, the cells were subsequently fixed with 4% formaldehyde, permeabilized with 0.1% Triton X-100 in PBS for 5 min. To confirm the purity of CMs and CFs isolated from mouse hearts, as well as NRCMs and NRCFs isolated from rat pups, cells were stained with troponin-T (1:500; MS-295-P1; Thermo Fisher Scientific, Waltham, MA, USA) and vimentin (1:500; ab45939; Abcam, Cambridge, MA, USA). The purity of isolated CMs (NRCMs) were verified by troponin-T positive staining and vimentin negative staining, conversely, the purity of isolated CFs (NRCFs) were verified by vimentin positive staining and troponin-T negative staining. To evaluate the surface area, cells were stained with phalloidin (1:50; ab143533; Abcam, Cambridge, MA, USA). To assess the expression and localization of specific proteins, the cells were stained with anti-FGF13 antibody (1:100; sc16811; Santa Cruz Biotechnology, Santa Cruz, CA, USA) or/and anti-NF-κB p65 (1:100; ab7970; Abcam, Cambridge, MA, USA) overnight. Finally, cells were incubated with Alexa Flour 647-conjugated donkey anti-goat antibody (1:250; ab150131; Abcam, Cambridge, MA, USA) or and Alexa Flour 488-conjugated donkey anti-rabbit antibody (1:250; ab150077; Abcam,

Cambridge, MA, USA) (or Alexa Flour 647-conjugated donkey anti-rabbit antibody (1:250; ab150075; Abcam, Cambridge, MA, USA)) at 4˚C overnight and nucleus were stained with 4,6 diamidino-2-phenylindole (DAPI) for 20 min. The cells were measured using Leica TCS SP5 Confocal microscope (Leica, Wetzlar, Germany).The surface areas were measured using Image-Pro Plus software, version 6.0.

## RNA isolation, semi-quantitative Reverse Transcriptase PCR and quantitative Real-Time Reverse Transcription PCR

Total RNA from cultured NRCMs or mouse hearts was isolated using TRIzol Reagent (15596018; Invitrogen, Carlsbad, CA, USA). cDNA was then synthesized using high capacity cDNA synthesis kit (4374967; Thermo Fisher Scientific, Waltham, MA, USA).

Subsequently, semi-quantitative Reverse Transcriptase PCR (sqRT-PCR) was conducted in Thermal Cycler (T100, Bio-Rad, Hercules, CA, USA). PCR signal intensity of each gene was electrophoresed in agarose gel, visualized by EtBr-Imaging (GelDoc XR+; Bio-Rad, Hercules, CA, USA). In addition, Quantitative real-time PCR (qRT-PCR) amplification of the indicated genes was performed using SYBR Green (04887352001, Roche). PCR thermal cycling involved a denaturing step at 95℃ for 10 min, followed by 45 cycles of annealing at 95℃ for 10 s, 60℃ for 10 s and 72℃ for 20 s. The target gene expression was normalized to GAPDH gene expression.

Gene-specific primer sequences used for PCR are listed as Supplementary Table 1.

### Extraction of cytoplasm and nucleus

Trypsinized cells were incubated in 500 µL of 0.1% NP-40/PBS for 5 minutes on ice and the reaction was stopped by adding 3 mL of cold PBS. Nucleus were isolated by centrifugation at 2000 rpm and washed with 3 mL of cold PBS twice. After washing, nucleus was lysed for 30 min in 50 mM Tris-HCl pH 7.5, 150 mM NaCl, 1% Nonidet P-40, 5 mM EGTA, 5 mM EDTA, 20 mM NaF and complete protease inhibitor cocktail (Roche Diagnostics, Indianapolis, IN). GAPDH and Lamin-b were used as the loading control for the cytoplasmic and the nuclear fraction, respectively.

## Western blot and Immunoprecipitation

The amount of 30 µg protein prepared from mouse hearts or NRCMs was used in a standard western blot analysis. The polyvinylidene fluoride (PVDF) membrane binding sample protein was incubated with a high affinity anti-FGF13 antibody (1:500; sc16811; Santa Cruz Biotechnology, Santa Cruz, CA, USA), anti-NF-κB p65 (1:1000; ab7970; Abcam, Cambridge, MA, USA), anti-p-IκBα (1:1000; sc8404; Santa

Cruz Biotechnology, Santa Cruz, CA, USA), anti-IκBα (1:1000; 4814; Cell Signaling Technology, Beverly, MA, USA), anti-IL-1β (1:2500; ab106035; Abcam, Cambridge, MA, USA), anti-IL-6 (1:1000; ab6672; Abcam, Cambridge, MA, USA), anti-Flag (1:1000; 8146; Cell Signaling Technology, Beverly, MA), anti-Myc (1:1000; 2278; Cell Signaling Technology, Beverly, MA, USA), anti-GAPDH antibody (1:2500; ab9485; Abcam, Cambridge, MA, USA), anti-Lamin-b (1:1000; 12586; Cell Signaling Technology, Beverly, MA, USA), respectively. Protein was visualized using the ECL Plus detection system (GE Healthcare, Waukesha, WI). The expressions of specific antigens were quantified using ImageQuant 5.2 software (Molecular Dynamics).

For immunoprecipitations, samples were precleared with 2 μg of normal goat immunoglobulin and 20 μL of Protein A/G beads (26147; Thermo Fisher Scientific, Waltham, MA, USA) for 1 h, and the precleared samples were incubated with the immobilized antibody at the concentrations as indicated. An aliquot of the precleared sample (one-tenth of the volume) before the immunoprecipitation reaction was designated as the input sample. After incubating for 2 h, 20 μL of Protein A/G beads were added for an additional 6 h. The beads were washed three times with lysing buffer and then eluted with sample buffer. For the immunodepletion experiments, the unbound samples in the supernatant from the bound beads were subsequently immunoprecipitated with the antibodies indicated in the figure legends. In some experiments, this process was repeated to immunodeplete multiple proteins from a single sample. The immunoprecipitates were subjected to immunoblotting using specific primary antibodies.

**Tricine-SDS-PAGE**

Tricine–SDS-PAGE is an efficient way of separating low molecular mass proteins. The assay was performed as described previously (Haider SR et al., 2019; Schägger H, 2006).

**Luciferase reporter assays in NRCMs**

Luciferase reporter assays from NRCMs were performed as described previously (Zhang Y et al., 2016). Ad-NFκB-luciferase reporter was obtained from Vector Biolabs (1740; Philadelphia, PA). Cells were cultured in 96-well plate and infected with adenovirus carrying NFκB-firefly-luciferase vector (1740; Vector Biolabs, Philadelphia, PA) at 100 multiplicity of infection. After incubation for the indicated time periods in the absence or presence of stimulators, the cell lysate was used for measurement of firefly luciferase activity with ONE-Glo luciferase assay system

(Promega, Madison, WI).

## Statistical analysis

Statistical analysis of the experimental data was performed using Graph Pad Prism 7.0 (GraphPad Software Inc., San Diego, CA, USA). Unpaired Student t test or one-way ANOVA with Turkey multiple comparison test was performed respective of the data type. Values were considered statistically significant if $P < 0.05$. All experiments were repeated at least three biological and technical repetitions and the data are presented as mean ± SEM unless noted otherwise.

## Supplemental References


Ackers-Johnson, M., Li, P.Y., Holmes, A.P., O'Brien, S.M., Pavlovic, D., and Foo, R.S. (2016). A Simplified, Langendorff-Free Method for Concomitant Isolation of Viable Cardiac Myocytes and Nonmyocytes From the Adult Mouse Heart. Circ Res 119:909-920.

Furihata, T., Kinugawa, S., Takada, S., Fukushima, A., Takahashi, M., Homma, T., Masaki, Y., Tsuda, M., Matsumoto, J., Mizushima, W., et al. (2016). The experimental model of transition from compensated cardiac hypertrophy to failure created by transverse aortic constriction in mice. Int J Cardiol Heart Vasc 11:24-28.

Haider, S. R., Reid, H. J., and Sharp, B. L. (2019). Tricine-SDS-PAGE. Methods in molecular biology (Clifton, N.J.) 1855:151-160.

Hulot, J.S., Fauconnier, J., Ramanujam, D., Chaanine, A., Aubart, F., Sassi, Y., Merkle, S., Cazorla, O., Ouillé, A., Dupuis, M., Hadri, L., et al. (2011). Critical role for stromal interaction molecule 1 in cardiac hypertrophy. Circulation 124:796-805.

Inagaki, K., Fuess, S., Storm, T.A., Gibson, G.A., Mctiernan, C.F., Kay, M.A., and Nakai, H. (2006). Robust systemic transduction with AAV9 vectors in mice: efficient global cardiac gene transfer superior to that of AAV8. Mol Ther 14:45-53.

McMullen, J.R., Shioi, T., Zhang, L., Tarnavski, O., Sherwood, M.C., Kang, P.M., and Izumo, S. (2003). Phosphoinositide 3-kinase (p110alpha) plays a critical role for the induction of physiological, but not pathological, cardiac hypertrophy. Proc. Natl. Acad. Sci. USA 100:12355-12360.

Pacak, C.A., Mah, C.S., Thattaliyath, B.D., Conlon, T.J., Lewis, M.A., Cloutier, D.E., Zolotukhin, I., Tarantal, A.F., and Byrne, B.J. (2006). Recombinant adeno-associated virus serotype 9 leads to preferential cardiac transduction in vivo. Circ Res 99:e3-e9.

Rockman, H.A., Ross, R.S., Harris, A.N., Knowlton, K.U., Steinhelper, M.E., Field, L.J., Ross, J, J.r., and Chien, K.R. (1991). Segregation of atrial-specific and inducible expression of an atrial natriuretic factor transgene in an in vivo murine model of cardiac hypertrophy. Proc Natl Acad Sci U S A 88:8277-8281.

Schägger H. (2006). Tricine-SDS-PAGE. Nature protocols 1:16-22.

Simpson, P. (1985). Stimulation of hypertrophy of cultured neonatal rat heart cells through an alpha 1-adrenergic receptor and induction of beating through an alpha 1- and beta 1-adrenergic receptor interaction. Evidence for independent regulation of growth and beating. Circ Res 56:884-894.

Suckau, L., Fechner, H., Chemaly, E., Krohn, S., Hadri, L., Kockskämper, J., Westermann, D., Bisping, E., Ly, H., Wang, X., et al. (2009). Long-term cardiac-targeted RNA interference for the treatment of heart failure restores cardiac function and reduces pathological hypertrophy. Circulation 119:1241-1252.

Vandergriff, A.C., Hensley, M.T., Cheng, K. (2015). Isolation and cryopreservation of neonatal rat cardiomyocytes. J Vis Exp.

Zhang, Y., Liu, J., Yao, S., Li, F., Xin, L., Lai, M., Bracchi-Ricard, V., Xu, H., Yen, W., Meng, W., et al. (2012). Nuclear factor kappa B signaling initiates early differentiation of neural stem cells. Stem Cells 30:510-524.

Zincarelli, C., Soltys, S., Rengo, G., and Rabinowitz, J.E. (2008). Analysis of AAV serotypes 1-9 mediated gene expression and tropism in mice after systemic injection. Mol Ther 16:1073-1080.

519 **Supplementary Table 1 Gene-specific primer sequences. Related to Figure 1-7;**
520 **Figure S1, S2, S9, S10**

| | |
|---|---|
| FGF13 (Mouse) | GGCAATGAACAGCGAGGGATACTTGTACAC |
| | CGGATTGCTGCTGACGGTAGATCATTGATG |
| FGF13 (Rat) | ACAAGCCTGCAGCTCATTTT |
| | CTTTTGCCCTCACTGGCTAC |
| ANF (Mouse) | TTGGCTTCCAGGCCATA |
| | AAGAGGGCAGATCTATCGGA |
| ANF (Rat) | AGCGGGGGCGGCACTTAG |
| | CTCCAATCCTGTCAATCC |
| BNP (Mouse) | GAGGTCACTCCTATCCTCTGG |
| | GCCATTTCCTCCGACTTTTCTC |
| BNP (Rat) | ATCGGCGCAGTCAGTCGCTT |
| | GGTGGTCCCAGAGCTGGGGAA |
| Collagen III (Mouse) | CCCAACCCAGAGATCCCATT |
| | GAAGCACAGGAGCAGGTGTAGA |
| Collagen III (Rat) | GCGGCTTTTCACCATATTAG |
| | GCATGT TTCTCCGGT TTC |
| Collagen I (Mouse) | AGGCTTCAGTGGTTTGGATG |
| | CACCAACAGCACCATCGTTA |
| Collagen I (Rat) | AACGATGGTGCCAAGGGTGAT |
| | ATTCTTGCCAGCAGGACCAAC |
| IL-6 (Mouse) | TGCTGGTGACAACCACGGC |
| | GTACTCCAGAAGACCAGAGG |
| IL-6 (Rat) | GACTTCACAGAGGATACCACCC |
| | CTCTGAATGACTCTGGCTTTGTC |
| IL-1β (Mouse) | ATGGCA ACTGTTCCTGAACTCAACT |

| | |
|---|---|
| | CAGGACAGGTATAGATTCTTTCCTTT |
| IL-1β (Rat) | CACCTCTCAAGCAGAGCACAG |
| | GGGTTCCATGGTGAAGTCAAC |
| GAPDH (Mouse) | ACTTGAAGGGTGGAGCCAAA |
| | GACTGTGGTCATGAGCCCTT |
| GAPDH (Rat) | GAAGGGTGGGGCCAAAAG |
| | GGATGCAGGGATGATGTTCT |
| Flag-FGF13 1-62 aa (human) | GAAATCCAACGCCTGCAAGT |
| | TGGAGCCGAAGAGTTTGACC |
| Flag-FGF13 63-214 aa (human) | AACCTCATCCCTGTGGGTCT |
| | CTGACTGCTGCTGACGGTAT |
| Flag-FGF13 215-245 aa (human) | CCCCAACCAAGAGCAGAAGT |
| | GTCGTCATCCTTGTAATCCGTTG |
| FGF13-S(mouse) | CGAGAAATCCAATGCCTGC |
| | CACCACCCGAAGACCCACAG |
| FGF13-U (mouse) | GTTAAGGAAGTCATATTCAGAGC |
| | CACCACCCGAAGACCCACAG |
| FGF13-V (mouse) | GCTTCTAAGGAGCCTCAGC |
| | CACCACCCGAAGACCCACAG |
| FGF13-VY (mouse) | GCTTCTAAGGTTCTGGATGAC |
| | CACCACCCGAAGACCCACAG |
| FGF13-VY/Y (mouse) | CACAGAACCCGAAGAGCCTCAG |
| | CACCACCCGAAGACCCACAG |

521